DETERMINATION OF LANDING ZONES OF QUADROTORS EXPERIENCING IN-FLIGHT FAILURES

by

AHMET TOLCU

THESIS

Submitted in partial fulfillment of the requirements
for the degree of Master of Science at
The University of Texas at Arlington
December, 2020

Arlington, Texas

Supervising Committee:

Animesh Chakravarthy, Supervising Professor
Atilla Doğan
Kamesh Subbarao

ACKNOWLEDGEMENTS

First and foremost, I would like to express the deepest gratitude to my supervisor Dr. Animesh Chakravarthy for his guidance and insight throughout the thesis study. It was a great honor to work with him for the last two years, and his effort influenced my academic career. He never hesitated to provide his opinions and feedback when I requested his help during my research. In addition, I offer my sincere appreciation to my co-supervisor Dr. Atilla Doğan for allowing me to have a master's degree at UTA and his academic support and Dr. Kamesh Subbarao for his participation to my thesis committee.

I wish to extend my utmost gratitude to the Republic of Turkey Ministry of National Education for providing me financial support during my graduate education. Thanks should also go to Tuncay Altun and Yusuf Kartal from the UTA Turkish Student Association for their support.

DEDICATION

I dedicate this thesis to my lovely family. I want to take this opportunity to express my heartiest gratitude to my dear mother and father, who have brought me to this day with their effort and patience, and to my dear brother and sister who have always given me joie de vivre.

Last but not least, I am tremendously grateful for Mustafa Tarık Asan's precious friendship, so much so that I cannot think of any appropriate words that could define his immense supports.

LIST OF FIGURES

ABSTRACT

DETERMINATION OF LANDING ZONES OF QUADROTORS EXPERIENCING IN-FLIGHT FAILURES

AHMET TOLCU, M.S.

The University of Texas at Arlington, December, 2020

Supervising Professor: Animesh Chakravarthy

Co-supervising Professor: Atilla Doğan

In recent years, unmanned aerial vehicles (UAVs), commonly known as drones, have attained considerable prominence in a wide range of areas ranging from military operations, including surveillance, intelligence, and reconnaissance, to nonmilitary sectors such as delivery, entertainment, and agriculture. The low cost, small size, and ease of use of quadrotors provide significant advantages for such missions. At the same time however, the occurrence of physical failures in such vehicles, particularly if these failures occur while flying over highly populated areas, can pose considerable risk to people and premises on the ground. This thesis investigates scenarios of power loss due to one or more rotor failures of a quadrotor and performs an analysis of the ensuing crash radius of the vehicle, occurring because of this power loss. The baseline controller of the vehicle is assumed to be a nonlinear controller designed using a dynamic inversion method. Four different failure scenarios are simulated, and a comparison of the crash radius obtained from simulation results and an analytical formulation is performed.

TABLE OF CONTENTS

CHAPTER 1

INTRODUCTION

1.1 Motivation

In recent years, unmanned aerial vehicles (UAVs), commonly known as drones, have been given extraordinary prominence in a wide range of areas from military operations, including surveillance, intelligence and reconnaissance with the features of stealth and low radar cross-section to nonmilitary sectors such as delivery, entertainment, agriculture. The UAVs are operated with different levels of autonomy from the remote control by an operator to autonomously onboard computers.

The UAVs can be categorized into two main groups based on wing shape: fixed-wing and rotary-wing. Rotary wing UAVs have some operational superiorities over fixed-wing by virtue of vertical take-off landing, hovering, and low-speed flight capabilities. These capabilities enable them to perform aggressive maneuvers in both indoors and outdoors environments. Furthermore, the robustness of these systems meets safety measurements in the course of high-risk operations in dangerous and restricted areas. Based on these criteria, many rotary-wing vehicles such as helicopters and quadrotors have gained importance over other aerial vehicles.

Quadrotors provide significant advantages compared with conventional VTOL vehicles such as helicopters because they are low cost, smaller in size and easier to use. In contrast, helicopters have greater mechanical complexity, but since quadrotors are mechanically more simple. They are popular among researchers, because they are easier to use in laboratories and can give real-time applications to confirm their studies. However, nonlinearity behaviors of these platforms' dynamics can be

seen as primary disadvantages. Therefore, the quadrotors need a reliable nonlinear controller to overcome this drawback and accomplish the mission demanding aggressive maneuvers and high accuracy.

The quadrotors are also appropriate testbeds to improve control techniques while performing a flight simulation for exposed uncertainties and disturbances. In this context, the essential part is to gauge the quadrotor orientation and position utilizing remarkable development in sensors, actuators, and other technological devices on the system.

On the other hand, these vehicles have a considerable risk to populated areas and properties on the ground due to possible physical failures. Therefore, this risk may cause several safety concerns for the public areas and it must be determined for risk assessment to get a nonhazardous flight. One of the risky conditions for a quadrotor is actuator failure while operating. This type of failure ends with a crash on the ground in parallel with the loss of power of the system. To develop a risk assessment for flight, the maximum crash radius should be calculated. In this thesis, the analytical approach is used to find the crash zone predetermined by flight conditions and the number of faulted rotors in several rates of power loss.

1.2 Literature Survey

The control methods for quadrotors should be addressed on a large scale since they have high order nonlinearities and complicated dynamic models. One of the factors that make the control more difficult for these vehicles is the underactuated characteristic specified to have fewer inputs than the degree of freedom [17]. Moreover, the strong coupling between rotational dynamics can be considered the crucial factor for position and orientation control problems. [11] The control algorithms can comprehensively be categorized into two groups as the linear and nonlinear ap-

proaches. The linearization proceeding is necessary for the equilibrium point to apply linear control methods.

The PID controller is a linear control algorithm and the most popular control scheme in the electrical and mechanical industry. In terms of adjusting the gain parameters, straightforward design, and easy implementation, this method is more advantageous than others for quadrotor platforms [23], [25]. But it has some disadvantages, such as performance limits due to nonlinearities related to the mathematical model [14]. For example, a PID controller was introduced for a quadrotor in [18] and [1] to track desired positions and orientations. The controller achieved effective performance to stabilize the system in ideal time with nearly zero steady-state error and modest overshoot. Although the PID controller has some performance limitations, it is broadly preferred by introducing the quadrotors in the literature. The tuning of this type of controller's gain parameters may cause some difficulties that require practice at the hovering position defined as the equilibrium point.

Furthermore in [12], the researchers discussed the remarkable deviations inflicting vehicle airframe and velocity while the quadrotor was hovering. They concluded that a proportional-derivative controller was adequate to stabilize for pitch motion but as velocity enhanced, the different measurements were necessary for blade flapping. Their work illustrated that the current control method was weak when using high-speed action and in windy experimental environments.

The optimal control algorithms act on linear dynamic systems by minimizing the cost performance index weighting coefficients sourced by the operator. In [2], researchers applied the linear quadratic regulator (LQR) on the structure and attained a performance comparison between PID and LQR. Both control techniques provided the same effect approximately; however, LQR performance is slightly better than PID in consideration that it was introduced as a more fully dynamic model.

For example, Cowling and coresearchers employed the LQR technique on a quadrotor's complete dynamic model for a path following in [8]. It was illustrated that despite there being wind and disturbance, the path following was attained precisely utilizing optimal trajectory. When the quadrotor tried to escape from an obstacle, it showed a tendency to lose tracking capability. The LQR method can be transformed into a Linear Quadratic Gaussian with a Kalman Filter for Gaussian noise and missing state data. The full state information is not necessary anymore with LQG implemented in [22] for quadrotor control.

Furthermore, to get better controller performance, nonlinear control methods were developed. One of the most rampant nonlinear control approaches is feedback linearization. This control method transforms the quadrotor platform's nonlinear system dynamics into a corresponding dynamic via change of variables on feedback rather than the small-angle approximation method. This technique requires exact models for application and has some loss of accuracy. It was used in a wide range of studies to design a flight controller. For example, Ghandour et al. presented a control scheme with this technique to make the platform follow a trajectory in the rotor faults circumstances in [13]. Additionally, D. Lee et al. developed a flight controller based on feedback linearization [16]. Their research pointed out that this controller technique is delicate to uncertainties and noise. Therefore, they neglected the disturbance and used small-angle deviation to abstain from elaborate differentiation terms. As a result, the researchers obtained results without disturbance in simulation by getting the gain parameters with the LQR technique.

Another study was presented on the basis of feedback linearization by Choi et al. practicing the controller used adaptive feedback linearization [7]. The quadrotor model uncertainties may deprive the task's achievement and can be obviated with an adaptation law to get essential modifications. In the same way, the adaptive

controller was designed in [5]. It can be seen that this method is sufficient for decreased error while tracking and increased operational performance. Consequently, nonlinear feedback linearization technique for control the quadrotor acts as well-being tracking but it is not efficient to reject disturbance. If applied with the combination of the alternative control algorithm, this shortcoming can be dealt with.

Backstepping control based on Lyapunov theory is one of the most popular nonlinear control methods that divide the controller steps using a recursive algorithm scheme to stabilize the sub-systems. Despite the low robustness and necessity of full state knowledge, this type of controller has certain superiorities, such as less computational load and its ability to considerably manage the disturbances. Because of these reasons, numerous researchers applied this strategy to design a quadrotor flight controller [10].

The research group implemented a backstepping controller in blocks with motor dynamics and obtained the trajectory following virtually [20]. The controller design in the [21] had a resemblance to [20]; however, the seventh block in [20] has consisted of motor rotational speeds despite the seventh block formed by forces in [21]. In [20], the optimum results are gained with a backstepping controller between five (applied) different controller methods. The stabilization and trajectory tracking tasks for quadrotor are accomplished with an integral backstepping technique terminating the sensor noise, external disturbances, and unmodelled effects [4].

For example, in [9], the research group presented a different form of the backstepping technique, and obtained the dynamics in the form Lagrangian instead of state-space representation. Due to the bilinearity of the Lagrangian position dynamics control in inverse kinematic, two neural networks are utilized to estimate aerodynamics moments and aerodynamic forces. Kartal et al. implemented a backstepping approach to design a PID controller and achieve guaranteed performance

later [15]. Firstly, to get this performance for micro UAV, the second order sliding variable is utilized in the backstepping design. The vehicle's nonlinear structure is then transformed into a PID controller with small-angle approximation and specific geometric manipulations.

The sliding mode control method is also a nonlinear control technique that works to change the system variables using a discontinuous input signal to the system to force it through an appointed path called sliding surface. This control algorithm does not need any simplification for dynamics. The control law switches in state- space from one state to another state using position information due to its location between control blocks. Bouabdallah and co-researchers proposed the sliding mode control, a sliding surface defined by the Lyapunov stability theory for managing the rotation subsystem in [3]. This control approach was matched with the backstepping algorithm and it was clearly illustrated that the SMC was not better than backstepping due to the switching operations in high frequency.

In [19], a quadrotor stabilization is obtained by active and passive fault-tolerant sliding mode controllers in the event of loss of effectiveness in a rotor. The sliding surface is described by the sum of error, the integral and derivative of errors. Although the sliding mode is good at eradicating external disturbance and model uncertainties, this controller design endures the issue of chattering. An active fault-tolerant controller is considered to give more suitable results than the passive fault-tolerant considering that there are two switching situations in the active one. In [24], error quaternion based on an adaptive sliding mode control scheme is proposed. This type of controller deals with disturbance and model inertia uncertainty.

The researchers compared a dynamic sliding mode controller with another controller based on the feedback linearization method in [6]. The dynamic sliding mode controller performs more effectively than feedback linearization at canceling the un-

known external disturbances. The system state responses approach the system's reference values accurately.

1.3 Thesis Outline

This thesis includes the mathematical model and a controller design of quadrotor and failure mode analysis to determine the crash zone. In chapter 2, the detailed model and fundamental motion concepts are introduced, and the section follows to derive the dynamic equations of this platform. In chapter 3, a nonlinear control method called dynamic inversion is discussed based on a mathematical approach and employed in the simulation platform. To calculate the crash zone resulting actuator power loss, the analytical approach is introduced considering the several failure scenarios in chapter 4. Finally, chapter 5 addresses the results that compare the simulation and analytical solutions of the failure scenarios.

CHAPTER 2

SYSTEM DYNAMICS & MODELLING

This chapter will discuss the detailed analysis of quadrotor dynamics and modeling starting with the fundamental motion concepts. The section then proceeds to describe the reference frames and rotation matrix that provide transformation for motion. In the next part, quadrotor rotational and translational dynamics equations are derived for the mathematical model. In the end, control inputs that are necessary for the controller section are defined under the control allocation section.

2.1 Fundamental Motion Concepts

The quadrotor is an underactuated aerial system with six degrees of freedom body moved by variation between the rotational speeds of the four rotors. Each rotor comprises a propeller with a certain number of blades that create the airflows downward to get lift force thanks to their design shape, no matter direction of their rotation.

The quadrotor can move only upward and downward as translational motion due to being an underactuated vehicle. The translational movements in the direction of x and y axes are related to the lift force coupled with rotation about all three axes. The lift force is generated as the total contribution of four rotors, and the torques about all three-axis called the roll, pitch, and yaw motions are produced due to different speeds between rotor pairs.

The four rotors can be grouped into two-part. The first group is the front and rear rotors (1 & 3) and produces pitch movement around the y-axis rotating

in a clockwise direction. The second group is the right and left rotors (2 & 4) and produces roll movement around the x-axis rotating in a counterclockwise direction.

The rotor pairs cause the yaw motion different than the roll and pitch moment rotating faster or slower than each other. Also, the rotor pairs virtually remove aerodynamic moments and gyroscopic effects rotating the opposite directions.

Quadrotor's fundamental motion concepts can be seen in Figure 1. The magnitude of each rotor propeller rotation speed is illustrated to be directly proportional to the width of the arrows in the figure.

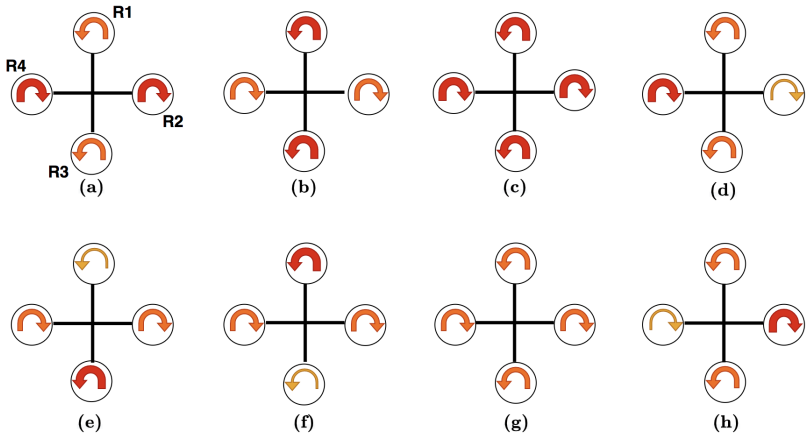

Figure 1. Fundamental motions of a quadrotor.

a – Yaw motion in the counterclockwise direction

b – Yaw motion in the clockwise direction

c – Take-off or hovering

d – Roll motion in the clockwise direction

e – Pitch motion in the counterclockwise direction

f – Pitch motion in the clockwise direction

g – Landing or descent

h – Roll motion in the counterclockwise direction

2.2 Reference Frames

To describe a quadrotor's position and orientation, it is necessary to specify some fundamental concepts before the mathematical model. A quadrotor has various sensors that have position and orientation data and outputs of these sensors are defined on a set of frames; earth-fixed and body-fixed frames. The gyro and accelerometer on the quadrotor measure data with respect to the body frame, whereas a GPS, required for position and ground speed, gives information in the earth-fixed frame.

The earth-fixed frame is located on the earth's surface, and the body frame is fixed to the center of gravity of the quadrotor's body, and it moves together with the quadrotor. As shown in Figure 2, the x_b and y_b axes are indicated to Rotor 1 and Rotor 2 direction, and ultimately the z_b axis is indicated vertically upward; that is the opposite way of the ground.

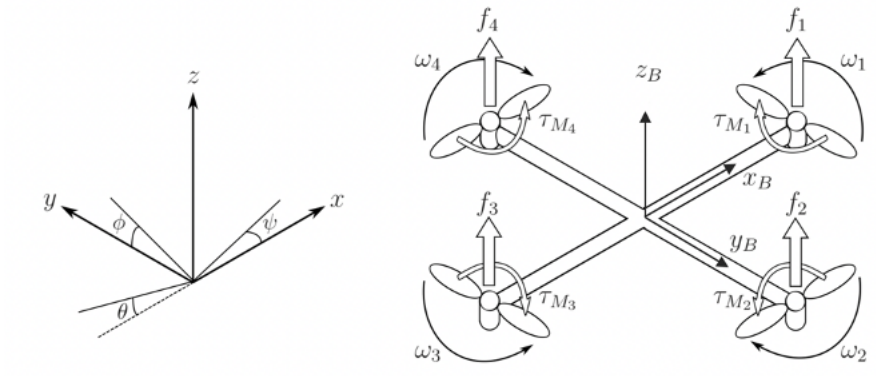

Figure 2. Earth-fixed and body-fixed reference frames.

2.3 Rotation Matrix

While modeling the quadrotor mathematically, equations of motions must be expressed on the same coordinate frame. The required transformations such as translation and rotation are developed between the frames using Euler angles and their rotation matrices. A rotation sequence of Euler angles $\psi - \theta - \phi$ can be utilized to achieve these transformations. The Euler angles are the rotation angles that enable the earth-fixed frame to coincide with the body frame. The following rotation matrices (2.1) are used respectively to represent the rotations around each axis, x, y, and z, as given in Figure 3.

$$R(\phi) = \begin{bmatrix} 1 & 0 & 0 \\ 0 & \cos\phi & -sin\phi \\ 0 & \sin\phi & \cos\phi \end{bmatrix} \tag{2.1a}$$

$$R(\theta) = \begin{bmatrix} \cos\theta & 0 & \sin\theta \\ 0 & 1 & 0 \\ -sin\theta & 0 & \cos\theta \end{bmatrix} \tag{2.1b}$$

$$R(\psi) = \begin{bmatrix} \cos\psi & -sin\psi & 0 \\ sin\psi & \cos\psi & 0 \\ 0 & 0 & 1 \end{bmatrix} \tag{2.1c}$$

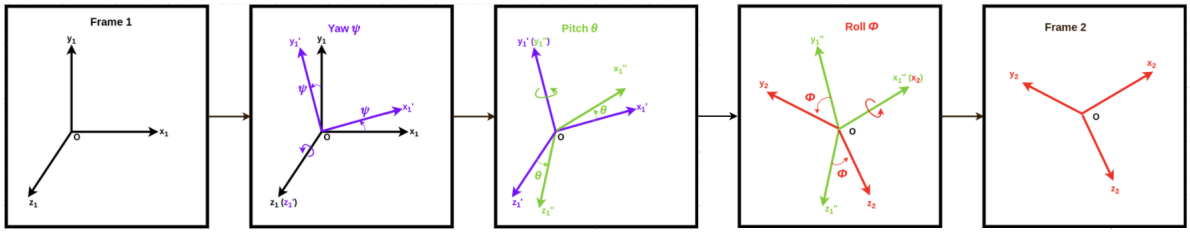

Figure 3. Euler angles.

The rotation matrix converting a vector from the body to the earth-fixed frame is constructed multiplying the matrices for each rotation and expressed as:

$$R_b^e = R(\psi)R(\theta)R(\phi) \tag{2.2}$$

$$R_b^e = \begin{bmatrix} \cos\psi\cos\theta & \sin\theta\cos\psi\sin\phi - \sin\psi\cos\phi & \cos\psi\sin\theta\cos\phi + \sin\psi\sin\phi \\ \sin\psi\cos\theta & \sin\psi\sin\theta\sin\phi + \cos\psi\cos\phi & \sin\psi\sin\theta\cos\phi - \sin\phi\cos\psi \\ -\sin\theta & \cos\theta\sin\phi & \cos\theta\cos\phi \end{bmatrix} \tag{2.3}$$

2.4 Mathematical Model

A convenient model should be designed to make a quadrotor fly smoothly in compliance with its structural properties. Quadrotors have strict requirements for developing controller approaches due to being nonlinear underactuated systems. At this stage, a rigorous dynamic model is a very critical cornerstone, because quite different outcomes in theory and practical implementations can result from differences between model and real dynamics. Considering the importance of these systems' dynamics, they must be modeled as meticulously as possible.

In this thesis, in order to derive the mathematical model of the vehicle by using the Newton-Euler technique, the following assumptions need to be made.

- The structure of the frame is rigid.
- The total mass is fixed, and the vehicle is symmetrical.
- The center of gravity coincides with the body frame.
- The earth is flat and the earth-fixed frame is accepted as inertial.
- The propeller of the rotors is rigid and not flapping.
- Drag and thrust forces are in proportion with the square of the speed of the rotors.
- Aerodynamic effects are neglected.

2.4.1 Kinematic Equations

2.4.1.1 Rotational Kinematics

The angular velocities of the quadrotor defined on the body frame are represented as $\omega = (p, q, r)$. These velocity rates can be measured using an Inertial Measurement Unit sensor, and they should be expressed with respect to Euler rates $\dot{\eta} = (\dot{\phi}, \dot{\theta}, \dot{\psi})$ by a series of rotation matrices using the transformation below because quadrotor makes a move on the earth's surface and the Euler angles and these angular body rates are different from each other.

$$\begin{bmatrix} p \\ q \\ r \end{bmatrix} = I \begin{bmatrix} \dot{\phi} \\ 0 \\ 0 \end{bmatrix} + R(\phi) \begin{bmatrix} 0 \\ \dot{\theta} \\ 0 \end{bmatrix} + R(\phi)R(\theta) \begin{bmatrix} 0 \\ 0 \\ \dot{\psi} \end{bmatrix} \tag{2.4}$$

Substituting x and y rotation matrices in equation (2.4)

$$\begin{bmatrix} p \\ q \\ r \end{bmatrix} = \begin{bmatrix} 1 & 0 & 0 \\ 0 & 1 & 0 \\ 0 & 0 & 1 \end{bmatrix} \begin{bmatrix} \dot{\phi} \\ 0 \\ 0 \end{bmatrix} + \begin{bmatrix} 1 & 0 & 0 \\ 0 & \cos\phi & -\sin\phi \\ 0 & \sin\phi & \cos\phi \end{bmatrix} \begin{bmatrix} 0 \\ \dot{\theta} \\ 0 \end{bmatrix} + \begin{bmatrix} 1 & 0 & 0 \\ 0 & \cos\phi & -\sin\phi \\ 0 & \sin\phi & \cos\phi \end{bmatrix} \begin{bmatrix} \cos\theta & 0 & \sin\theta \\ 0 & 1 & 0 \\ -\sin\theta & 0 & \cos\theta \end{bmatrix} \begin{bmatrix} 0 \\ 0 \\ \dot{\psi} \end{bmatrix} \tag{2.5}$$

$$\begin{bmatrix} p \\ q \\ r \end{bmatrix} = \begin{bmatrix} 1 & 0 & -\sin\theta \\ 0 & \cos\phi & \sin\phi\cos\theta \\ 0 & -\sin\phi & \cos\phi\cos\theta \end{bmatrix} \begin{bmatrix} \dot{\phi} \\ \dot{\theta} \\ \dot{\psi} \end{bmatrix} \tag{2.6}$$

$$\begin{bmatrix} \dot{\phi} \\ \dot{\theta} \\ \dot{\psi} \end{bmatrix} = \begin{bmatrix} 1 & \sin\phi\tan\theta & \tan\theta\cos\phi \\ 0 & \cos\phi & -\sin\phi \\ 0 & \sin\phi\sec\theta & \cos\phi\sec\theta \end{bmatrix} \begin{bmatrix} p \\ q \\ r \end{bmatrix} \tag{2.7}$$

The quadrotor performs its motion mostly in hovering with small angles. Therefore, angular velocities may be considered equal as the Euler angles rates with small-angle assumptions. ($\dot{\phi} \cong p, \dot{\theta} \cong q, \dot{\psi} \cong r$)

2.4.1.2 Translational Kinematics

The linear velocities defined on the body frame are represented as $\nu = (u, v, w)$ and these can be transformed to linear velocities on the earth-fixed frame, $\dot{r} = (\dot{x}, \dot{y}, \dot{z})$ using the rotation matrix.

$$\dot{r} = R_b^e \nu \tag{2.8}$$

$$\begin{bmatrix} \dot{x} \\ \dot{y} \\ \dot{z} \end{bmatrix} = \begin{bmatrix} \cos\psi\cos\theta & \sin\theta\cos\psi\sin\phi - \sin\psi\cos\phi & \cos\psi\sin\theta\cos\phi + \sin\psi\sin\phi \\ \sin\psi\cos\theta & \sin\psi\sin\theta\sin\phi + \cos\psi\cos\phi & \sin\psi\sin\theta\cos\phi - \sin\phi\cos\psi \\ -\sin\theta & \cos\theta\sin\phi & \cos\theta\cos\phi \end{bmatrix} \begin{bmatrix} u \\ v \\ w \end{bmatrix} \tag{2.9}$$

2.4.2 Dynamic Equations

2.4.2.1 Translational Dynamics

Translational dynamics are obtained by the linear momentum change dependent on Newton's second law. By this law, the rate of change of linear momentum of a rigid body is proportional to the force applied. In equation (2.10), F_e is the total force affecting the quadrotor, m is the mass and $\dot{r}$ is the linear velocity vector on the earth-fixed frame.

$$F_e = m\frac{d\dot{r}}{dt} \tag{2.10}$$

Due to all forces acting on the body frame, the equation (2.10) can be expressed as below on the body frame.

$$F_b = m\dot{\nu} + \omega \times m\nu \tag{2.11}$$

$$\begin{bmatrix} F_{xb} \\ F_{yb} \\ F_{zb} \end{bmatrix} = m \begin{bmatrix} \dot{u} \\ \dot{v} \\ \dot{w} \end{bmatrix} + \begin{bmatrix} p \\ q \\ r \end{bmatrix} \times m \begin{bmatrix} u \\ v \\ w \end{bmatrix} \tag{2.12}$$

The unbalanced external forces defined in the equation (2.13) acting on the vehicle cause translational accelerations.

$$F_b = T - (R_b^e)^T F_g \tag{2.13}$$

where F_g is gravitational force and T is the total thrust force required for flight. In the quadrotor system, the total thrust force is produced by four rotors which generate one-directional separate thrust force, T_i.

$$T_i = k\Omega_i^2, i = 1, 2, 3, 4 \tag{2.14}$$

where k is the thrust factor defining the relation thrust and rotational speed of the rotor.

$$T = T_1 + T_2 + T_3 + T_4 = k(\Omega_1^2 + \Omega_2^2 + \Omega_3^2 + \Omega_4^2) \tag{2.15}$$

The transformation can be obtained between forces on the earth-fixed and body frames utilizing the rotation matrix.

$$\begin{bmatrix} F_{xe} \\ F_{ye} \\ F_{ze} \end{bmatrix} = R_b^e \begin{bmatrix} F_{xb} \\ F_{yb} \\ F_{zb} \end{bmatrix} = R_b^e \begin{bmatrix} 0 \\ 0 \\ T \end{bmatrix} - m \begin{bmatrix} 0 \\ 0 \\ g \end{bmatrix} = m \begin{bmatrix} \ddot{x}_e \\ \ddot{y}_e \\ \ddot{z}_e \end{bmatrix} \tag{2.16}$$

$$\begin{bmatrix} \ddot{x}_e \\ \ddot{y}_e \\ \ddot{z}_e \end{bmatrix} = \begin{bmatrix} (\cos\phi \sin\theta \cos\psi + \sin\phi \sin\psi)\frac{T}{m} \\ (\cos\phi \sin\theta \sin\psi - \sin\phi \cos\psi)\frac{T}{m} \\ (\cos\phi \cos\theta)\frac{T}{m} - g \end{bmatrix} \tag{2.17}$$

2.4.2.2 Rotational Dynamics

Rotational dynamics are revealed by the angular momentum change from the motions around the quadrotor's center of gravity. Equations of the rotational dynamics are derived as below.

$$M_e = I\frac{d\omega_e}{dt} \tag{2.18}$$

which ends up with the form of Euler's equation

$$M_e = I\dot{\omega}_e + \omega_e \times I\omega_e \tag{2.19}$$

where M_e is the moment acting on the quadrotor, I and ω_e represent the inertia matrix of the structure and the angular velocity matrix, respectively, on the earth-fixed frame. Due to all moments acting on the body frame, the equation (2.19) can be expressed below on the body frame utilizing the rotation matrix

$$M = I\dot{\omega} + \omega \times I\omega \tag{2.20}$$

where the inertia matrix is diagonal resulting from the symmetrical structure and given by

$$I = \begin{bmatrix} I_x & 0 & 0 \\ 0 & I_y & 0 \\ 0 & 0 & I_z \end{bmatrix} \tag{2.21}$$

and the moment vector on the body frame is

$$M = \begin{bmatrix} L \\ M \\ N \end{bmatrix} \tag{2.22}$$

where L,M and N are the roll, pitch and yaw moments, respectively.

$$\begin{bmatrix} L \\ M \\ N \end{bmatrix} = \begin{bmatrix} I_x & 0 & 0 \\ 0 & I_y & 0 \\ 0 & 0 & I_z \end{bmatrix} \begin{bmatrix} \dot{p} \\ \dot{q} \\ \dot{r} \end{bmatrix} + \begin{bmatrix} p \\ q \\ r \end{bmatrix} \begin{bmatrix} I_x & 0 & 0 \\ 0 & I_y & 0 \\ 0 & 0 & I_z \end{bmatrix} \begin{bmatrix} p \\ q \\ r \end{bmatrix} \tag{2.23}$$

Using equation (2.6), the moment on the body frame can be represented on the earth frame with respect to Euler angles and their rates as shown in equation (2.24) where s denotes sin function, c denotes cos function.

$$\begin{bmatrix} L \\ M \\ N \end{bmatrix} = \begin{bmatrix} I_x(\ddot{\phi} - s\theta\ddot{\psi} - c\theta\dot{\theta}\dot{\psi}) + (I_z - I_y)(c\phi\dot{\theta} + s\phi c\theta\dot{\psi})(s\phi\dot{\theta} - c\phi c\theta\dot{\psi}) \\ I_y(c\phi\ddot{\theta} + s\phi c\theta\ddot{\psi} - s\phi\dot{\phi}\dot{\theta} + c\phi c\theta\dot{\phi}\dot{\psi} - s\phi s\theta\dot{\theta}\dot{\psi}) + (I_z - I_x)(s\phi\dot{\theta} - c\phi c\theta\dot{\psi})(\dot{\phi} - s\theta\dot{\psi}) \\ I_z(-s\phi\ddot{\theta} + c\phi c\theta\ddot{\psi} - c\phi\dot{\phi}\dot{\theta} - s\phi c\theta\dot{\phi}\dot{\psi} - c\phi s\theta\dot{\theta}\dot{\psi}) + (I_x - I_y)(c\phi\dot{\theta} + s\phi c\theta\dot{\psi})(\dot{\phi} - s\theta\dot{\psi} \end{bmatrix} \tag{2.24}$$

Assuming that the quadrotor mostly hovers and tends to orientate with the small angles while in flight, we can simplify the equation (2.24) as below.

$$\begin{bmatrix} L \\ M \\ N \end{bmatrix} = \begin{bmatrix} I_x\ddot{\phi} + (I_z - I_y)\dot{\theta}\dot{\psi} \\ I_y\ddot{\theta} + (I_z - I_x)\dot{\phi}\dot{\psi} \\ I_z\ddot{\psi} + (I_x - I_y)\dot{\phi}\dot{\theta} \end{bmatrix} \tag{2.25}$$

The moments are produced with the thrust forces generated by each rotor. The moment about x_b axis is called roll moment with rotating of the Rotor 2 and Rotor 4 at different rotational speeds. Similarly, Rotor 1 and Rotor 3 create the moment called pitch moment about y_b axis.

The thrust forces generated by the rotor pairs (R1-R3 and R2-R4) cause a moment difference between x_b and y_b axes proportional to air drag by rotating clockwise and counterclockwise directions. With the result of this drag force, a moment is produced about z_b axis called yaw moment.

$$M_\phi = -lT_2 + lT_4 = lk(-\Omega_2^2 + \Omega_4^2) \tag{2.26a}$$

$$M_\theta = -lT_1 + lT_3 = lk(-\Omega_1^2 + \Omega_3^2) \tag{2.26b}$$

$$M_\psi = -M_1 + M_2 - M_3 + M_4 = d(-\Omega_1^2 + \Omega_2^2 - \Omega_3^2 + \Omega_4^2) \tag{2.26c}$$

where l represents the distance between the rotor's midpoint and quadrotor's center of gravity and d is the drag factor.

$$\begin{bmatrix} \ddot{\phi} \\ \ddot{\theta} \\ \ddot{\psi} \end{bmatrix} = \begin{bmatrix} \dot{\theta}\dot{\psi}((I_y - I_z) + M_\phi)/I_x \\ \dot{\phi}\dot{\psi}((I_x - I_z) + M_\theta)/I_y \\ \dot{\phi}\dot{\theta}((I_y - I_x) + M_\psi)/I_z \end{bmatrix} \tag{2.27}$$

2.5 Control Inputs Allocation

The left sides of the equation (2.12) and (2.25) include applied force and moments of the quadrotor on the body frame. Therefore, these terms can be used to get inputs in the system. To achieve desired outputs such as angular and linear velocities on the body frame, the required thrusts for each rotor must be commanded

in accordance with the desired inputs utilizing these equations. The control inputs can be obtained with the following equations.

$$\begin{bmatrix} T \\ M_\phi \\ M_\theta \\ M_\psi \end{bmatrix} = \begin{bmatrix} T_1 + T_2 + T_3 + T_4 \\ -lT_2 + lT_4 \\ -lT_1 + lT_3 \\ -M_1 + M_2 - M_3 + M_4 \end{bmatrix} = \begin{bmatrix} k(\Omega_1^2 + \Omega_2^2 + \Omega_3^2 + \Omega_4^2) \\ lk(-\Omega_2^2 + \Omega_4^2) \\ lk(-\Omega_1^2 + \Omega_3^2) \\ d(-\Omega_1^2 + \Omega_2^2 - \Omega_3^2 + \Omega_4^2) \end{bmatrix} = \begin{bmatrix} k(u_1 + u_2 + u_3 + u_4) \\ lk(-u_2 + u_4) \\ lk(-u_1 + u_3) \\ d(-u_1 + u_2 - u_3 + u_4) \end{bmatrix} \tag{2.28}$$

The equation (2.28) shows that there are linear relationships between inputs and the moments and the thrust. Hence, to normalize the moments and thrust with regard to the input u, the pseudo inputs vector, u^*, can be defined as in equation (2.29) and the connection between the actual input and pseudo input is represented as in equation (2.30):

$$u^* = [u_{ver} \ , \ u_{roll} \ , \ u_{pitch} \ , \ u_{yaw}]^T \tag{2.29}$$

$$\begin{bmatrix} u_{ver} \\ u_{roll} \\ u_{pitch} \\ u_{yaw} \end{bmatrix} = \begin{bmatrix} T/k \\ M_\phi/kl \\ M_\theta/kl \\ M_\psi/d \end{bmatrix} = \begin{bmatrix} 1 & 1 & 1 & 1 \\ 0 & -1 & 0 & 1 \\ -1 & 0 & 1 & 0 \\ -1 & 1 & -1 & 1 \end{bmatrix} \begin{bmatrix} u_1 \\ u_2 \\ u_3 \\ u_4 \end{bmatrix} \tag{2.30}$$

To create the motion in exact directions, utilizing the pseudo inputs allows a convenient method to control the vehicle. u_{ver} is the input that enables to ascend or descend of the quadrotor and u_{roll} , u_{pitch} and u_{yaw} are the inputs to produce roll, pitch and yaw motion, respectively.

Furthermore, to perform the desired movement, each rotor's desired rotational speed can be found in terms of the given inputs in the equation (2.31):

$$\begin{bmatrix} \Omega_1^2 \\ \Omega_2^2 \\ \Omega_3^2 \\ \Omega_4^2 \end{bmatrix} = \begin{bmatrix} \frac{1}{4k} & 0 & -\frac{1}{2k} & -\frac{1}{4d} \\ \frac{1}{4k} & -\frac{1}{2k} & 0 & \frac{1}{4d} \\ \frac{1}{4k} & 0 & \frac{1}{2k} & -\frac{1}{4d} \\ \frac{1}{4k} & \frac{1}{2k} & 0 & \frac{1}{4d} \end{bmatrix} \begin{bmatrix} u_{ver} \\ u_{roll} \\ u_{pitch} \\ u_{yaw} \end{bmatrix} \tag{2.31}$$

2.6 State - Space Representation

In this stage, the state-space representation of the quadrotor is given model dynamics in previous sections. The mathematical dynamic equations show that the quadrotor platform is a nonlinear system with multiple inputs and multiple outputs as in many modern systems. This situation makes understanding the system more complicated and time-consuming. To reduce the designer's load and to examine such a system, a state-space representation is used to express the internal dynamics of the system, namely state variables, with first-order differential equations.

The inputs created by the rotors and the outputs that are the movements of the system for each degree of freedom are represented with u and y vectors in equation (2.32) and (2.33):

$$u = [u_1, u_2, u_3, u_4]^T \tag{2.32}$$

$$y = [x, y, z, \phi, \theta, \psi]^T \tag{2.33}$$

The mapping between the described input and output is crucial in understanding the quadrotor system behaviors. The dynamic model and the measurement model of the vehicle can be defined in the equation (2.34) and (2.35):

$$\dot{x}(t) = f(x(t)) + g(x(t))u(t) \tag{2.34}$$

$$y(t) = h(x(t)) \tag{2.35}$$

We can define the quadrotor body response with models described in equation (2.17) and equation (2.29). The system states are obtained as below:

$$y = [x, y, z, \phi, \theta, \psi, \dot{x}, \dot{y}, \dot{z}, \dot{\phi}, \dot{\theta}, \dot{\psi}]^T \tag{2.36}$$

The whole model is then defined in full by

$$\ddot{r} = \frac{1}{m} R_b^e \begin{bmatrix} 0 \\ 0 \\ ku_{ver} \end{bmatrix} - \begin{bmatrix} 0 \\ 0 \\ g \end{bmatrix} \tag{2.37}$$

$$\ddot{\eta} = I^{-1} \left(\begin{bmatrix} klu_{roll} \\ klu_{pitch} \\ du_{yaw} \end{bmatrix} - \dot{\eta} \times I\dot{\eta} \right) \tag{2.38}$$

CHAPTER 3

CONTROL STRATEGY

The physical systems generally have inherent nonlinear and coupled dynamics. For this reason, the systems need to be controlled by nonlinear techniques to deal with the nonlinearities' aspects during the missions. These nonlinear methods can be obtained by making dynamic inversion or defining the nonlinear system with nonlinear form. This chapter will discuss the dynamic inversion method employed in the quadrotor dynamics in the simulation environment.

3.1 Nonlinear Dynamic Inversion

The dynamic inversion method has been one of the most rampant nonlinear control approaches dealing with the nonlinear system, regarded as if it is linear to control. This process can be considered a linearization type, but it differs entirely from classical Jacobian linearization that utilizes the dynamics' approximations. This method obtains algebraically a coordinate transformation of nonlinear states to get a linear feedback law between inputs and outputs. To apply the linear control notion and achieve a mission such as tracking the trajectory or stabilizing the system, it is crucial to find applicable state transformation. Before proceeding with the dynamic inversion control strategy, some concepts about this control technique should be discussed.

3.1.1 The Relative Degree

Considering a nonlinear single input – single output (SISO) system of the form

$$\dot{x} = f(x) + g(x)u \tag{3.1a}$$

$$y = h\left(x\right) \tag{3.1b}$$

where $x \in \mathbb{R}^n$, u and y are scalars, $g\left(x\right)$ is a single vector field and $h\left(x\right)$ is a scalar function. Then

$$\dot{y} = \frac{\partial h}{\partial x}.\frac{\partial x}{\partial t} = \frac{\partial h}{\partial x}\left(f\left(x\right) + g\left(x\right)u\right) = L_f h + L_g h u \tag{3.2}$$

If $L_g h = 0$, there will not be the input variable in the output equation. This means that the input does not have any effect in a given x_0 that desired point for a regulator or system trajectory. For that reason, the taking derivative of y should be repeated until the output has the input u explicitly.

Continuing the taking derivatives in that condition:

$$y = h(x) \tag{3.3a}$$

$$\dot{y} = L_f^1 h + L_g h u = L_f^1 h \; with \; L_g h = 0 \tag{3.3b}$$

$$\ddot{y} = L_f^2 h + L_g(L_f^1 h)u = L_f^2 h \; with \; L_g h = 0 \tag{3.3c}$$

$$\vdots$$

$$y^r = L_f^r h + L_g(L_f^{r-1} h)u = v \; with \; L_g h \neq 0 \tag{3.3d}$$

The number r represents the term called the relative degree of $y = h(x)$ if and only if

$$L_g(L_f^{r-1}h) \neq 0 \tag{3.4}$$

In other words, the relative degree is the lowest step number that the coefficient of the input, u , is nonzero in the $\mathbb{R}^n$ space where is to be controlled.

To find the relative degree for nonlinear multi input – multi output systems (MIMO), let's define $f(x)$ and $g(x)$ are vector fields and γ is a scalar real-valued function. The Lie derivatives that contain derivations of $\gamma(x)$ along the $f(x)$ and $g(x)$ are attained as follows:

$$L_f\gamma(x) = \frac{\partial\gamma(x)}{\partial x}.f(x) = \left[\frac{\partial\gamma(x)}{\partial x_1} \ \ldots \ \frac{\partial\gamma(x)}{\partial x_n}\right].f(x) \tag{3.5}$$

$$L_f^k\gamma(x) = \frac{\partial(L_f^{k-1}\gamma(x))}{\partial x}.f(x) \tag{3.6}$$

$$L_gL_f\gamma(x) = \frac{\partial(L_f\gamma(x))}{\partial x}.g(x) \tag{3.7}$$

If $G(x) = [g_1(x) \ \ldots \ g_m(x)]$, introduced the Lie derivative on this function, we have:

$$L_G\gamma(x) = [L_{g1}\gamma(x) \ \ldots \ L_{gm}\gamma(x) \tag{3.8}$$

After formulating the fundamentals of Lie derivatives, the MIMO systems' relative degree can be obtained as follow:

$$\dot{y}_i = \frac{\partial y_i}{\partial x} = \frac{\partial h_i}{\partial x}.\frac{\partial x}{\partial t} = \frac{\partial h_i}{\partial x}.f\left(x\right) + \frac{\partial h_i}{\partial x}.G\left(x\right)u = L_f h_i\left(x\right) + L_G h_i\left(x\right)u = L_f h_i\left(x\right) \tag{3.9a}$$

$$\ddot{y}_i = \frac{\partial \dot{y}_i}{\partial x}.\frac{\partial x}{\partial t} = \frac{\partial L_f h_i}{\partial x}.\frac{\partial x}{\partial t} = \frac{\partial L_f h_i}{\partial x}.f\left(x\right) + \frac{\partial L_f h_i}{\partial x}.G\left(x\right)u = L_f^2 h_i\left(x\right) + L_G L_f h_i\left(x\right)u = L_f^2 h_i\left(x\right) \tag{3.9b}$$

$$\vdots$$

$$y_i^{r_i} = \frac{\partial y_i^{r_i-1}}{\partial x}.\frac{\partial x}{\partial t} = \frac{\partial L_f^{r_i-1} h_i}{\partial x}.\frac{\partial x}{\partial t} = \frac{\partial L_f^{r_i-1} h_i}{\partial x}.f\left(x\right) + \frac{\partial L_f^{r_i-1} h_i}{\partial x}.G\left(x\right) \tag{3.9c}$$

$$y_i^{r_i} = L_f^{r_i-1} h_i\left(x\right) + L_G L_f^{r_i-1} h_i\left(x\right)u \; with \; L_G L_f^{r_i-1} h_i\left(x\right) \neq 0 \tag{3.9d}$$

Summarizing the output dynamics as below:

$$y_i^{r_i} = B\left(x\right) + A\left(x\right)u \tag{3.10}$$

where

$$B\left(x\right) = \begin{bmatrix} L_f^{r_1} h_1 \\ L_f^{r_2} h_2 \\ \vdots \\ L_f^{r_m} h_m \end{bmatrix} \; and \; A\left(x\right) = \begin{bmatrix} L_{g1} L_f^{r_1-1} h_1 & L_{g2} L_f^{r_1-1} h_1 & \dots & L_{gm} L_f^{r_1-1} h_1 \\ L_{g1} L_f^{r_2-1} h_2 & L_{g2} L_f^{r_2-1} h_2 & \dots & L_{gm} L_f^{r_2-1} h_2 \\ \vdots & \vdots & \ddots & \vdots \\ L_{g1} L_f^{r_m-1} h_m & L_{g2} L_f^{r_m-1} h_m & \dots & L_{gm} L_f^{m-1} h_m \end{bmatrix} \tag{3.11}$$

The total relative degree for a MIMO system is in the form of $[r_1 \ \ldots \ r_m]$ vector at x_0 point and is found for the entire system by summing of each output's relative degree. It must be less than or equal to the order of the nonlinear system.

$$r = \sum_{r=1}^{m} r_i \leq n \tag{3.12}$$

One of the relative degree's crucial properties is to define the singularity of the $A(x)$ matrix, which is also called the decoupling matrix. Thus, the invertibility of this matrix is assured by the relative degree vector. If there is a relative degree vector existing, then $A(x)$, describing the matrix is invertible.

3.1.2 The System Transformation

In this section, the Lie derivatives will be used to obtain the state transformation. This transformation consists of replacing the original state variables x with the new state variables z (linearizing state) in the new state space. Every output y_i has a relative degree r_i and this output does not have any control input in the first $r_i - 1$ derivatives due to $L_g L_f^k h = 0$ on condition that $k \leq r - 1$. When $1 \leq k \leq m$, the subsequent transformation is defined for $1 \leq j \leq r_k$ Defining the function $T_j(x)$ as

$$z_j = T_j(x) = L_f^{j-1} h_k(x) \tag{3.13}$$

Applying the equation, the entire system can be converted into the following transformation:

$$\begin{bmatrix} z_1 \\ z_2 \\ \vdots \\ z_{r_1+\ldots+r_{m-1}+1} \\ \vdots \\ z_r \end{bmatrix} = \begin{bmatrix} y_1^0 \\ \vdots \\ y_1^{r_1-1} \\ \vdots \\ y_m^0 \\ \vdots \\ y_m^{r_m-1} \end{bmatrix} = \begin{bmatrix} L_f^0 h_1 \\ \vdots \\ L_f^{r_1-1} h_1 \\ \vdots \\ L_f^0 h_m \\ \vdots \\ L_f^{r_m-1} h_m \end{bmatrix} \tag{3.14}$$

The whole state transformation is represented by $z = T(x)$. The inverse is given by $x = T^{-1}(z)$.

$$z = T(x) \rightarrow x = T^{-1}(z) \tag{3.15}$$

Finally, nonlinear system dynamics can be transformed into an equivalent linear system dynamic exploiting these properties.

3.1.3 Feedback Linearization

At the essence of the dynamic inversion is the feedback linearization loop converting the nonlinear MIMO system model into a system consisting of decoupled integrators. For that reason, the dynamic inversion has stipulated the selection of input variables. To introduce this concept, the set of control variables can be stated in the following:

$$y_i^{r_i} = B(x) + A(x)\, u \tag{3.16}$$

$$\upsilon = B(x) + A(x)\, u \tag{3.17}$$

υ is the new control variable called the virtual control variable and necessary for the expression of the transformed system.

Solving for the input vector u, then the equation (3.18) is attained

$$u = A(x)^{-1}(\upsilon - B(x)) \tag{3.18}$$

When equation (3.18) is substituted into equation (3.17), the linear relation in equation (3.19) is obtained between output and the virtual input.

$$[y_1^{r_1} \ \cdots \ y_m^{r_m}]^T = [\upsilon_1 \ \cdots \ \upsilon_m]^T \tag{3.19}$$

In this way, the output's nonlinear and coupled dynamics are replaced with decoupled integrators between virtual control variables that correspond to outputs. The resulting linear system is controlled with a feedback law that operates on output's elements. The virtual input is defined as the desired output r th derivative of y in this closed-loop system. The sections related thus far will be made use of to design controllers in this thesis.

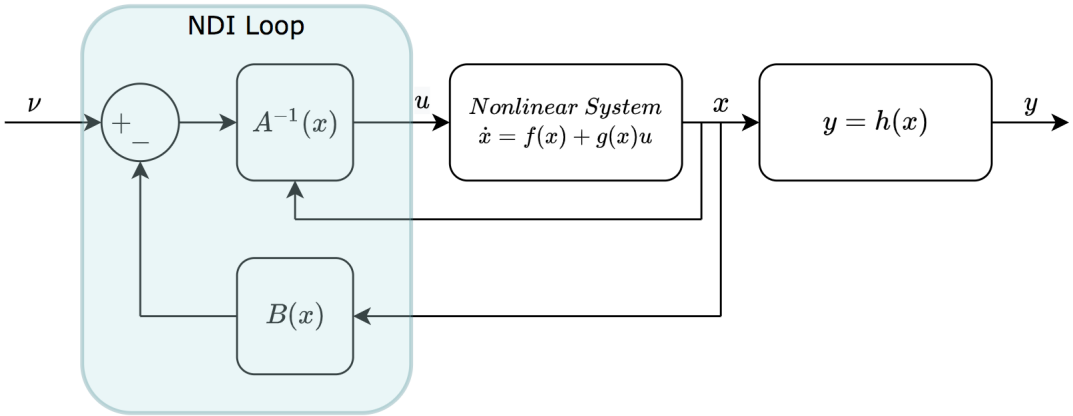

Figure 4. Feedback linearization block diagram.

3.2 Controller Design

To design an elegant controller using the nonlinear dynamic inversion method for the quadrotor, the control architecture is divided into two main loops called the inner and outer loop, which are nested based on two sets of outputs. The inner loop's objective is to stabilize the quadrotor's attitude receiving the desired roll, pitch, yaw angles, and control the height taking the total thrust generated by all rotors. On the other hand, the outer loop aims to allow the quadrotor to obtain the desired horizontal positions autonomously in the earth-fixed frame.

The inner loop outputs are defined as $y_i = [z\ \phi\ \theta\ \psi]^T$, and each element of this output vector can be controlled with separate inputs, $u^* = [u_{ver}\ ,\ u_{roll}\ ,\ u_{pitch}\ ,\ u_{yaw}]^T$ by the nature of the quadrotor. As a result, the inversion between these outputs and the virtual inputs, $\upsilon^* = [\upsilon_{ver}\ ,\ \upsilon_{roll}\ ,\ \upsilon_{pitch}\ ,\ \upsilon_{yaw}]^T$ can be derived with a linear relation. Then, a feedback law enables controlling the quadrotor's attitudes and height, determining the desired outputs.

To have appeared the control inputs in the output variables, the output must be differentiated as much as the order relative degree. For quadrotor dynamics, it can be seen that the relative degree is two as equations (2.39) and (2.40)

$$\ddot{z} = \frac{k}{m} u_{ver}\ \ (\cos\phi \cos\theta) - g \tag{3.20a}$$

$$\ddot{\phi} = \frac{kl}{I_x} u_{roll} + \frac{(I_z - I_y)}{I_x} \dot{\theta}\dot{\psi} \tag{3.20b}$$

$$\ddot{\theta} = \frac{kl}{I_y} u_{pitch} + \frac{(I_z - I_x)}{I_y} \dot{\phi}\dot{\psi} \tag{3.20c}$$

$$\ddot{\psi} = \frac{d}{I_z} u_{yaw} + \frac{(I_x - I_y)}{I_z} \dot{\phi}\dot{\theta} \tag{3.20d}$$

It is quite apparent that, the output is in the form of the equation (3.16) for the inner loop where

$$B(x) = \begin{bmatrix} -g \\ \frac{(I_z - I_y)}{I_x}\dot{\theta}\dot{\psi} \\ \frac{(I_z - I_x)}{I_y}\dot{\phi}\dot{\psi} \\ \frac{(I_x - I_y)}{I_z}\dot{\phi}\dot{\theta} \end{bmatrix}, \; A(x) = \begin{bmatrix} \frac{k}{m}(\cos\phi\cos\theta) & 0 & 0 & 0 \\ 0 & \frac{kl}{I_x} & 0 & 0 \\ 0 & 0 & \frac{kl}{I_y} & 0 \\ 0 & 0 & 0 & \frac{d}{I_z} \end{bmatrix}, \; u = \begin{bmatrix} u_{ver} \\ u_{roll} \\ u_{pitch} \\ u_{yaw} \end{bmatrix} \tag{3.21}$$

Applying the dynamic inversion method using equation (3.18)

$$u_{ver} = \frac{m}{k(\cos\phi\cos\theta)}(\upsilon_{ver} + g) \tag{3.22a}$$

$$u_{roll} = \frac{I_x}{kl}\left(\upsilon_{roll} + \frac{(I_y - I_z)}{I_x}\dot{\theta}\dot{\psi}\right) \tag{3.22b}$$

$$u_{pitch} = \frac{I_y}{kl}\left(\upsilon_{pitch} + \frac{(I_x - I_z)}{I_y}\dot{\phi}\dot{\psi}\right) \tag{3.22c}$$

$$u_{yaw} = \frac{I_z}{d}\left(\upsilon_{yaw} + \frac{(I_y - I_x)}{I_z}\dot{\phi}\dot{\theta}\right) \tag{3.22d}$$

After deriving the dynamic inversion, each virtual input should be mapped to the desired outputs for attitude and height control (3.22).

$$\upsilon^* = \begin{bmatrix} \upsilon_{ver} \\ \upsilon_{roll} \\ \upsilon_{pitch} \\ \upsilon_{yaw} \end{bmatrix} = \begin{bmatrix} \ddot{z} \\ \ddot{\phi} \\ \ddot{\theta} \\ \ddot{\psi} \end{bmatrix} \tag{3.23}$$

The linear feedback laws may then be employed to follow these linearized feedback dynamics in the following forms.

$$\begin{bmatrix} \upsilon_{ver} \\ \upsilon_{roll} \\ \upsilon_{pitch} \\ \upsilon_{yaw} \end{bmatrix} = \begin{bmatrix} \ddot{z}_{des} - K_{1z}\left(\dot{z} - \dot{z}_{des}\right) - K_{2z}\left(z - z_{des}\right) \\ \ddot{\phi}_{des} - K_{1\phi}\left(\dot{\phi} - \dot{\phi}_{des}\right) - K_{2\phi}\left(\phi - \phi_{des}\right) \\ \ddot{\theta}_{des} - K_{1\theta}\left(\dot{\theta} - \dot{\theta}_{des}\right) - K_{2\theta}\left(\theta - \theta_{des}\right) \\ \ddot{\psi}_{des} - K_{1\psi}\left(\dot{\psi} - \dot{\psi}_{des}\right) - K_{2\psi}\left(\psi - \psi_{des}\right) \end{bmatrix} \tag{3.24}$$

K_1 and K_2 gains should be selected positively for the error dynamics poles to be on the left-hand side of the s-plane. Thus, the inner loop may be stabilized with this controller. To assure the desired trajectory control, it is also required that the zero dynamics of the system defined by internal states (x and y) should be stabilized. It is achieved by obtaining the desired roll and pitch angle commands in terms of the desired dynamics of the horizontal accelerations in the equation (3.24) and (3.25).

$$\ddot{x} = \left(\cos\phi \sin\theta \cos\psi + \sin\phi \sin\psi\right) \frac{k}{m} u_{ver} \tag{3.25}$$

$$\ddot{y} = \left(\cos\phi \sin\theta \sin\psi - \sin\phi \cos\psi\right) \frac{k}{m} u_{ver} \tag{3.26}$$

To obtain ϕ_{des} and θ_{des} the horizontal acceleration dynamics equation may be inverted as the following

$$\phi_{des} = \arcsin\left(\frac{m(\ddot{x}\sin\psi - \ddot{y}\cos\psi)}{k u_{ver}}\right) \tag{3.27}$$

$$\theta_{des} = \arcsin\left(\frac{m(\ddot{x}\cos\psi + \ddot{y}\sin\psi)}{k u_{ver}\cos\phi}\right) \tag{3.28}$$

For desired x and y accelerations, the feedback laws can be attained with the same linear approach as the inner loop on the condition that there is instantaneous response of roll and pitch angles.

$$\ddot{x} = \ddot{x}_{des} - K_{1x}(\dot{x} - \dot{x}_{des}) - K_{2x}(x - x_{des}) \tag{3.29}$$

$$\ddot{y} = \ddot{y}_{des} - K_{1y}(\dot{y} - \dot{y}_{des}) - K_{2y}(y - y_{des}) \tag{3.30}$$

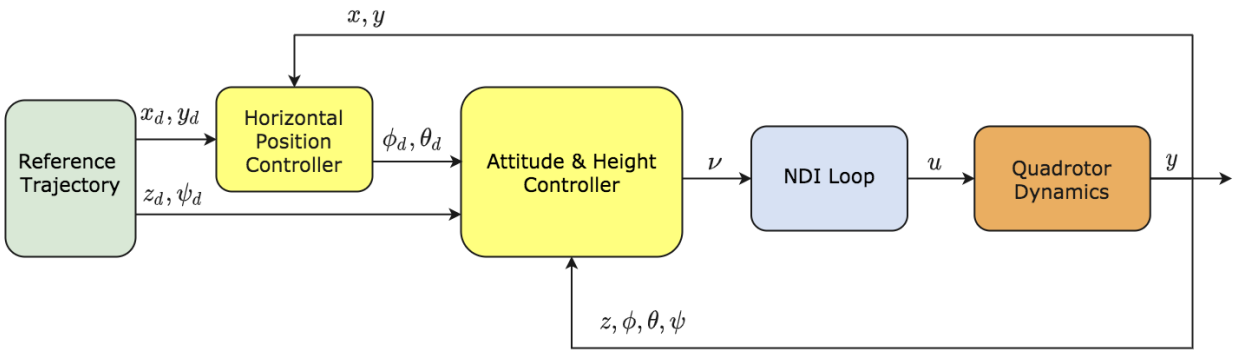

Figure 5. Controller design with dynamic inversion.

Figure 6. and Figure 7. present results for a circular trajectory response of controller designed with a dynamic inversion method. Figure 6. indicates a three-dimensional illustration of the quadrotor's path. The quadrotor is expected to take off from origin and move 1 m in the z-axis and perform a pitch maneuver to go 1 m in the x-axis. Then it draws a circle with both pitch and roll maneuvers. Finally,

the quadrotor completes its motion by landing 1 m far away from the origin in the x-axis.

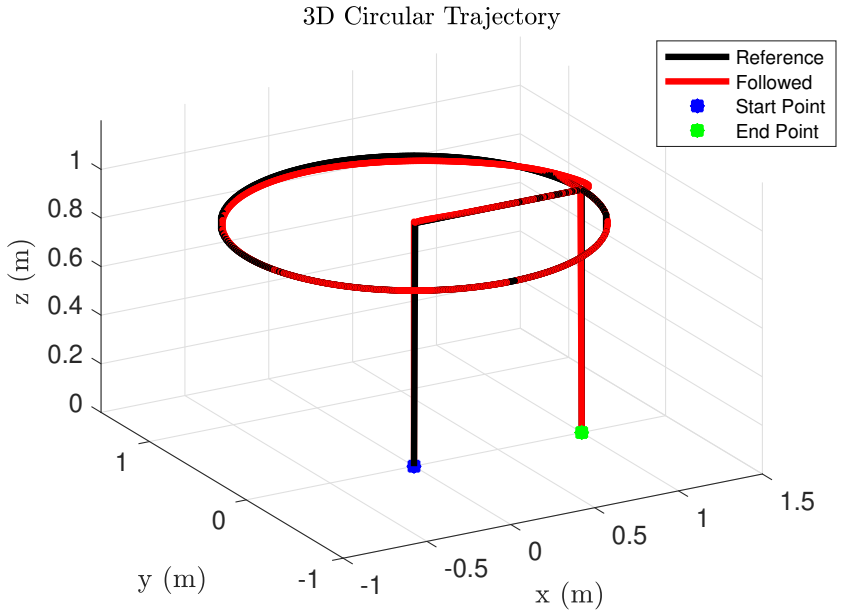

Figure 6. Following the 3d circular trajectory.

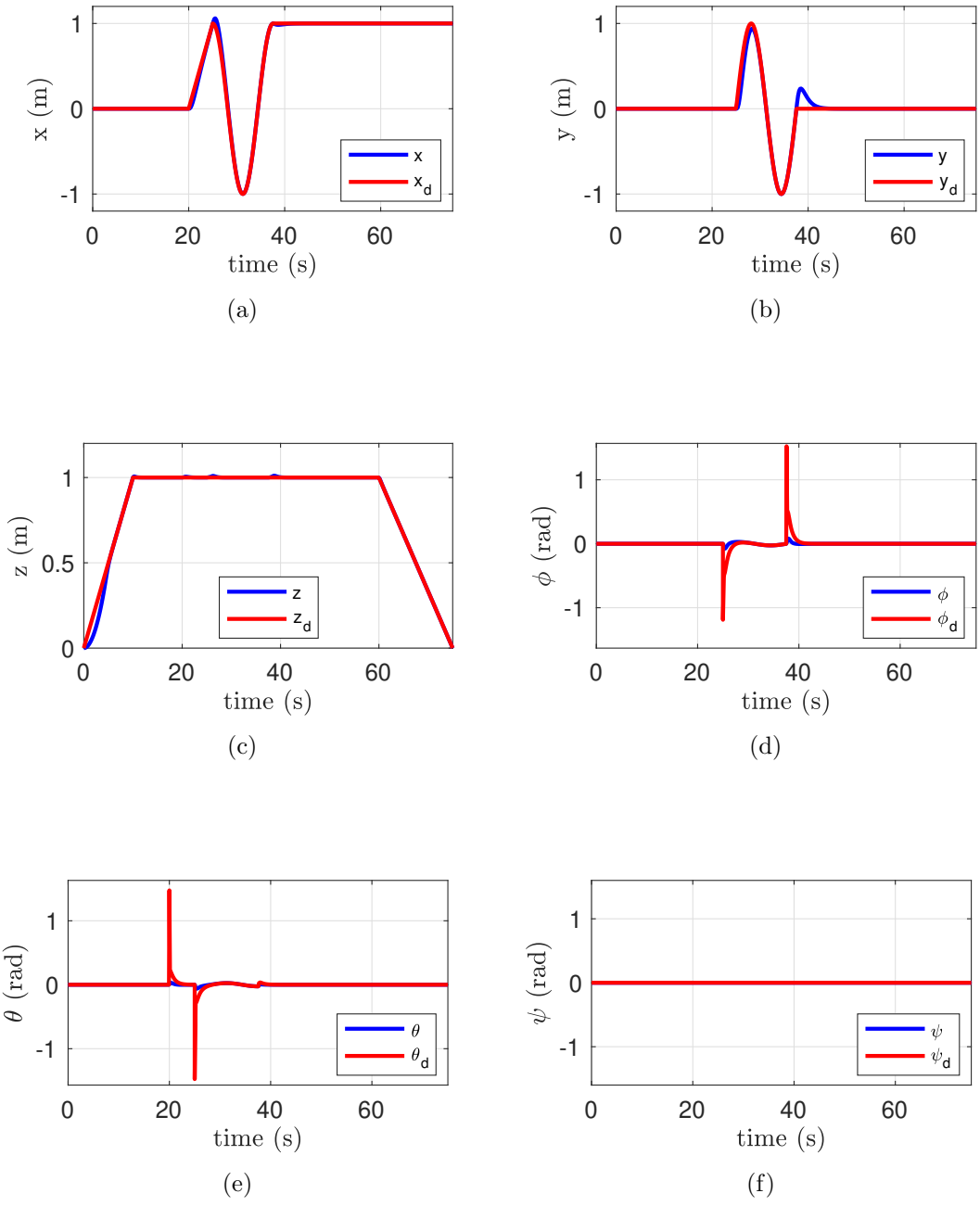

Figure 7. x, y, z positions and ϕ, θ, ψ angles tracking responses .

CHAPTER 4

ANALYTICAL SOLUTION

In this section, a study of the crash radius of the quadrotor is presented based on loss of effectiveness resulting from actuator failures, considering specific scenarios in the nonlinear simulation environment. The reason for the crash analysis is that the rotors contain both control surfaces and thrust mechanism. The rotor failures caused by propeller loss or other physical faults result in a persistent interruption in system capability.

The prediction of the crash position on the ground requires probabilistic and deterministic models. In this thesis, a deterministic model is utilized to find the landing zone using an analytical approach and disregarding the dynamic model uncertainties. It has been accepted that certain amounts of power loss in rotors cause deviations in the system dynamics. Based on these deviations, the trajectories to the impact point on the ground are obtained, making use of the small perturbation theory.

4.1 The Small Perturbation Theory

The quadrotor equations of motion are highly nonlinear, and it may be challenging to get exact solutions. In view of the problem's complexity, the linearization of these equations creates particularly desirable simplifications. The small perturbation theory brings about this linearization, which yields satisfactory results for far-reaching applications. The small perturbation theory is based on the simple method. Deviations from the previous steady states are defined by a small perturbed state

in the form of Taylor series for dynamic motion variables. These expressions are linearized by excluding high-order terms assuming that the products of two small perturbation terms are always negligible.

Assuming a simple first-order nonlinear system given as

$$\dot{x} = f(x) \tag{4.1}$$

The f function can be expressed performing Taylor expansion at an operating point x_0

$$f(x) = \sum_{n=0}^{\infty} \frac{f^{(n)}(x_0)}{n!}(x - x_0)^n = f(x_0) + \frac{f^{(1)}(x - x_0)}{1!} + \frac{f^{(2)}(x - x_0)^2}{2!} + \frac{f^{(3)}(x - x_0)^3}{3!} + \dots \tag{4.2}$$

Then, defining the deviation as $\Delta x = x - x_0$ which is an extremely small quantity from the operating point. Therefore, high-order terms can be negligible for this perturbation.

$$f(x) \approx f(x_0) + f^{(1)}(x - x_0) \tag{4.3}$$

After describing the change in output as $\Delta f(x) = f(x) - f(x_0)$, the equation (4.3) can be written as below

$$\Delta f(x) \approx f^{(1)}(x_0)\,\Delta x \tag{4.4}$$

$f^{(1)}(x_0)$ is a constant value; therefore, the nonlinear system approaches a linear system around the operating point. The operating point is determined at the quadrotor's hovering motion for linearization. Linear and rotational velocities and Euler

angles are considered as constant values at hovering motion. The small perturbation theorem can be applied in line with this knowledge for the quadrotor platform.

4.2 Analytical Solution

Designing the controller for the quadrotor, the error function is considered given as

$$e = y_{actual} - y_{desired} \tag{4.5}$$

When the power loss occurs on the system, a deviation is comprised of due to the failure. The deviation term is added to equation (4.5)

$$y_{actual} = e + y_{desired} + \Delta y \tag{4.6}$$

To calculate the deviation term the following steps are introduced. The dynamic equation for roll motion is given in equation (4.7)

$$\ddot{\phi} = \left(\dot{\theta}\dot{\psi}\left((I_z - I_y) + M_\phi\right)\right)/I_x \tag{4.7}$$

The quadrotor is a steady-state condition at hovering and roll acceleration is equal to zero.

$$\ddot{\phi_0} = 0 = \left(\dot{\theta_0}\ \dot{\psi}_0\left((I_z - I_y) + M_{\phi 0}\right)\right)/I_x \tag{4.8}$$

Defining the small displacement identities for each variable for roll moment dynamics in (4.9)

$$\dot{\phi} = \dot{\phi_0} + \Delta\dot{\phi},\ \dot{\theta} = \dot{\theta_0} + \Delta\dot{\theta},\ \dot{\psi} = \ \dot{\psi}_0 + \Delta\dot{\psi},\ \ddot{\phi} = \ddot{\phi_0} + \Delta\ddot{\phi},\ M_\phi = M_{\phi 0} + \Delta M_\phi \tag{4.9}$$

Substituting the identities into the equation (4.7)

$$\ddot{\phi}_0 + \Delta\ddot{\phi} = \left(\left(\dot{\theta}_0 + \Delta\dot{\theta}\right)\left(\dot{\psi}_0 + \Delta\dot{\psi}\right)(I_z - I_y) + (M_{\phi 0} + \Delta M_\phi)\right)/I_x \tag{4.10}$$

Note that $\ddot{\phi}_0 = 0$ and the product of two small disturbance terms are very small and Euler rates are zero. Therefore, equation (4.9) becomes

$$\Delta\ddot{\phi} = \frac{\Delta M_\phi}{I_x} \Rightarrow \Delta\dot{\phi} = \frac{\Delta M_\phi}{I_x}t \Rightarrow \Delta\phi = \frac{\Delta M_\phi}{2I_x}\Delta t^2 \tag{4.11}$$

The equation (4.12) and (4.13) are obtained with the same procedure for pitch and yaw motions.

$$\Delta\ddot{\theta} = \frac{\Delta M_\theta}{I_y} \Rightarrow \Delta\dot{\theta} = \frac{\Delta M_\theta}{I_y}t \Rightarrow \Delta\theta = \frac{\Delta M_\theta}{2I_y}\ \Delta t^2 \tag{4.12}$$

$$\Delta\ddot{\psi} = \frac{\Delta M_\psi}{I_z} \Rightarrow \Delta\dot{\psi} = \frac{\Delta M_\psi}{I_z}t \Rightarrow \Delta\psi = \frac{\Delta M_\psi}{2I_z}\Delta t^2 \tag{4.13}$$

To calculate the deviation in the direction of the x-axis and y-axis, the steps are followed below with the assumption that there is not yaw motion while designing the controller.

$$\ddot{x} = \frac{T}{m}\left(\cos\phi\sin\theta\cos\psi + \sin\phi\sin\psi\right) \Rightarrow \ddot{x} = \frac{T}{m}\left(\cos\phi\sin\theta\right) \tag{4.14}$$

Substituting the small displacement identities into the equation (4.14)

$$\ddot{x}_0 + \Delta\ddot{x} = \left(\frac{T_0 + \Delta T}{m}\right)[\cos(\phi_0 + \Delta\phi)\sin(\theta_0 + \Delta\theta)] \tag{4.15}$$

We use trigonometric identities in (4.15) and consider $I_x = I_y$ due to the symmetric structure of the vehicle.

$$\begin{aligned}\ddot{x}_0 + \Delta\ddot{x} = \left(\frac{T_0 + \Delta T}{2m}\right)[&\sin(\phi_0 + \theta_0)\cos(\left(\frac{\Delta M_\phi + \Delta M_\theta}{2I_x}\right)\Delta t^2) \\ &+ \cos(\phi_0 + \theta_0)\sin(\left(\frac{\Delta M_\phi + \Delta M_\theta}{2I_x}\right)\Delta t^2) \\ &- \sin(\phi_0 - \theta_0)\cos(\left(\frac{\Delta M_\phi - \Delta M_\theta}{2I_x}\right)\Delta t^2) \\ &- \cos(\phi_0 - \theta_0)\sin(\left(\frac{\Delta M_\phi - \Delta M_\theta}{2I_x}\right)\Delta t^2)]\end{aligned} \tag{4.16}$$

The Taylor expansions are used instead of trigonometric functions in (4.16) and this equation is integrated two times to find the deviation on the x-axis.

$$\begin{aligned}x_0 + \Delta x = \left(\frac{T_0 + \Delta T}{2m}\right)[&\sin(\phi_0 + \theta_0)\sum_n^\infty \frac{(-1)^n a^{2n}(\Delta t)^{4n+2}}{(2n)!\,(4n+1)(4n+2)} \\ &+ \cos(\phi_0 + \theta_0)\sum_n^\infty \frac{(-1)^n a^{2n+1}(\Delta t)^{4n+4}}{(2n+1)!\,(4n+3)(4n+4)} \\ &- \sin(\phi_0 - \theta_0)\sum_n^\infty \frac{(-1)^n b^{2n}(\Delta t)^{4n+2}}{(2n)!\,(4n+1)(4n+2)} \\ &- \cos(\phi_0 - \theta_0)\sum_n^\infty \frac{(-1)^n b^{2n+1}(\Delta t)^{4n+4}}{(2n+1)!\,(4n+3)(4n+4)}]\end{aligned} \tag{4.17}$$

where ϕ_0 and θ_0 are initial angles while starting the failure and $a = \dfrac{\Delta M_\phi + \Delta M_\theta}{2I_x}$, $b = \dfrac{\Delta M_\phi - \Delta M_\theta}{2I_x}$

The same method is used to find the deviation on the y-axis with the assumption that there is not yaw motion.

$$\ddot{y} = \frac{T}{m}\left(\cos\phi \sin\theta \sin\psi - \sin\phi \cos\psi\right) \Rightarrow \ddot{y} = \frac{T}{m}\left(-\sin\phi\right) \tag{4.18}$$

Substituting the small displacement identities into the equation (4.18)

$$\ddot{y}_0 + \Delta\ddot{y} = -\left(\frac{T_0 + \Delta T}{m}\right)\sin(\phi_0 + \Delta\phi) \quad = -\left(\frac{T_0 + \Delta T}{m}\right)\left[\sin\phi_0 \cos\Delta\phi + \cos\phi_0 \sin\Delta\phi\right] \tag{4.19}$$

Considering $c = \dfrac{\Delta M_\phi}{2I_x}$ and integrating two times the equation (4.19), we have equation (4.20) for y-axis deviation in Taylor expansion form.

$$\begin{aligned} y_0 + \Delta y = -\left(\frac{T_0 + \Delta T}{m}\right)\Big[\sin\phi_0 \sum_{n=0}^{\infty} \frac{(-1)^n c^{2n} (\Delta t)^{4n+2}}{(2n)!\,(4n+1)\,(4n+2)} \\ + \cos\phi_0 \sum_{n=0}^{\infty} \frac{(-1)^n c^{2n+1} (\Delta t)^{4n+4}}{(2n+1)!\,(4n+3)\,(4n+4)}\Big] \end{aligned} \tag{4.20}$$

To find the radius of the landing zone, the equation (4.21) is derived using Δx and Δy.

$$r = \sqrt{(x_0 + \Delta x)^2 + (y_0 + \Delta y)^2} \tag{4.21}$$

One of the objectives of this thesis is to get the landing zone depending for the certain power loss rate of the rotors on the quadrotor. Before proceeding, the relation between the rotor power and rotor rotational speed should be expressed in equation (4.22) below:

$$P = \tau\Omega \tag{4.22}$$

where P is power, τ is torque and Ω is rotational speed of the rotor.

In the following discussion, it is assumed that the net torque is constant to attain necessary lift force for quadrotor. Therefore, it can be seen that the decrese amount of the rotational speed of rotor is proportional to rate of the power loss due to physical failures since the landing zone analysis is based on the power loss of the rotors.

The failure scenarios are designed according to assumptions on the fault of Rotor 1 and the fault of both Rotor 1 and 2 at the same rate of power loss. In line with this knowledge, the equations (2.15) and (2.26) can be converted to find the deviations of thrust and moments as below:

The case of Rotor 1 failure:

$$T_0 + \Delta T = k((\Omega_1 - \Delta\Omega_1)^2 + \Omega_2^2 + \Omega_3^2 + \Omega_4^2) \tag{4.23}$$

$$M_{\phi 0} = lk(-\Omega_2^2 + \Omega_4^2) \tag{4.24}$$

$$M_{\theta 0} + \Delta M_\theta = lk(-(\Omega_1 - \Delta\Omega_1)^2 + \Omega_3^2) \tag{4.25}$$

$$M_{\psi 0} + \Delta M_\psi = d(-(\Omega_1 - \Delta\Omega_1)^2 + \Omega_2^2 - \Omega_3^2 + \Omega_4^2) \tag{4.26}$$

The case of both Rotor 1 and Rotor 2 failures at the same rates and time:

$$T_0 + \Delta T = k((\Omega_1 - \Delta\Omega_1)^2 + (\Omega_2 - \Delta\Omega_2)^2 + \Omega_3^2 + \Omega_4^2) \tag{4.27}$$

$$M_{\phi 0} + \Delta M_\phi = lk(-(\Omega_2 - \Delta\Omega_2)^2 + \Omega_4^2) \tag{4.28}$$

$$M_{\theta 0} + \Delta M_\theta = lk(-(\Omega_1 - \Delta\Omega_1)^2 + \Omega_3^2) \tag{4.29}$$

$$M_{\psi 0} + \Delta M_\psi = d(-(\Omega_1 - \Delta\Omega_1)^2 + (\Omega_2 - \Delta\Omega_2)^2 - \Omega_3^2 + \Omega_4^2) \tag{4.30}$$

CHAPTER 5

SIMULATION RESULTS

5.1 Failure Scenarios

In this study, four different failure scenarios are simulated and solved analytically using the 3d circular trajectory in Figure 6. These scenarios can be categorized into two groups as maneuvering and hovering flight depend on the number of failured rotors on the quadrotor. The scenarios can be summarized with their conditions as below.

- Scenario 1: Rotor-1 Failure in hovering flight

  $\phi_0 = 0$, $\theta_0 = 0$ and $\Delta M_\phi = 0$, $\Delta M_\theta \neq 0$
- Scenario 2: Rotor-1 and Rotor-2 Failures in hovering flight

  $\phi_0 = 0$, $\theta_0 = 0$ and $\Delta M_\phi \neq 0$, $\Delta M_\theta \neq 0$
- Scenario 3: Rotor-1 Failure in maneuvering flight

  $\phi_0 \neq 0$, $\theta_0 \neq 0$ and $\Delta M_\phi = 0$, $\Delta M_\theta \neq 0$
- Scenario 4: Rotor-1 and Rotor-2 Failures in maneuvering flight

  $\phi_0 \neq 0$, $\theta_0 \neq 0$ and $\Delta M_\phi \neq 0$, $\Delta M_\theta \neq 0$

5.2 Scenario 1 Results

It is assumed that the quadrotor's number 1 rotor is exposed the power loss at the time of 65 s of hovering flight. The deviation trajectories are obtained based on the power loss rate and the crash zone is shown.

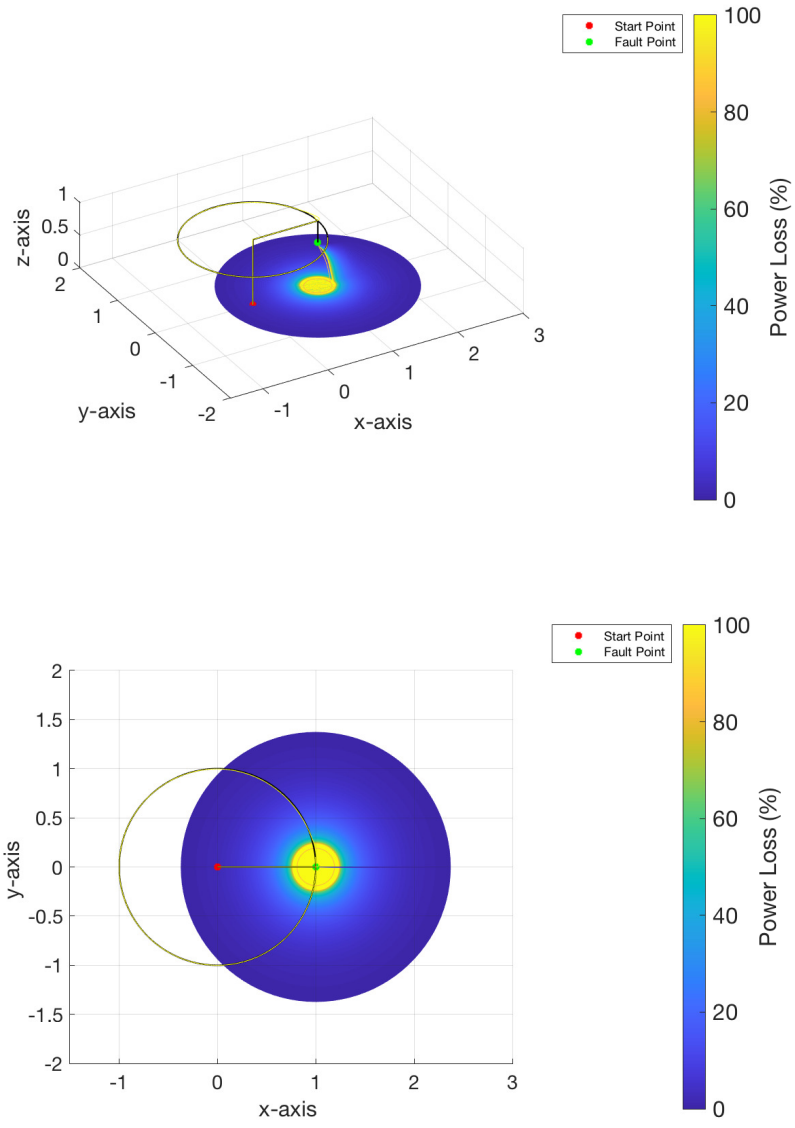

Figure 8. 3d and top views for crash zone in scenario 1.

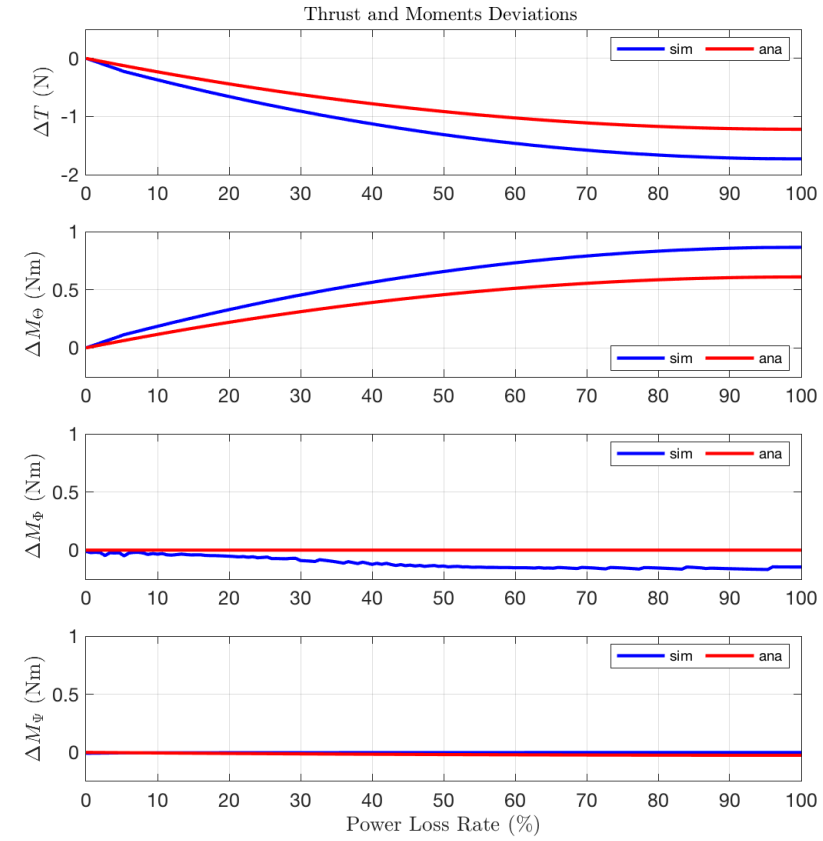

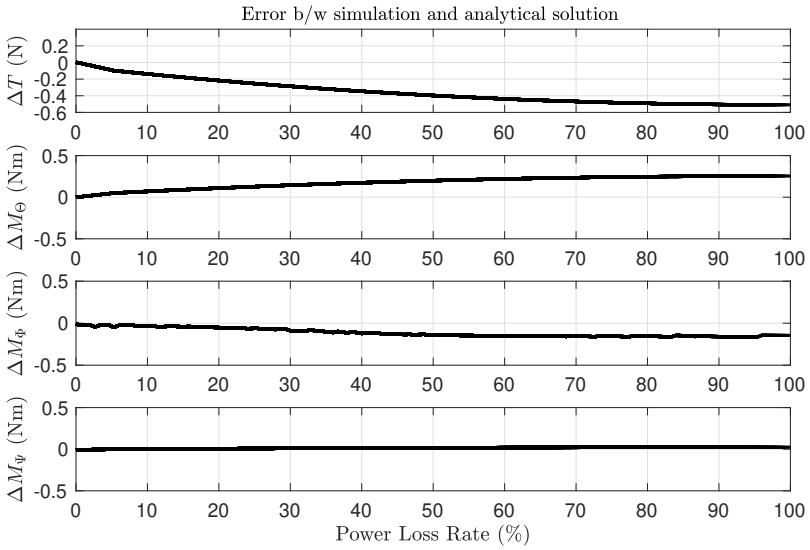

Figure 9. Thrust & moments deviations vs power loss of Rotor 1 in hovering flight and errors b/w simulation and analytical solution for scenario 1 .

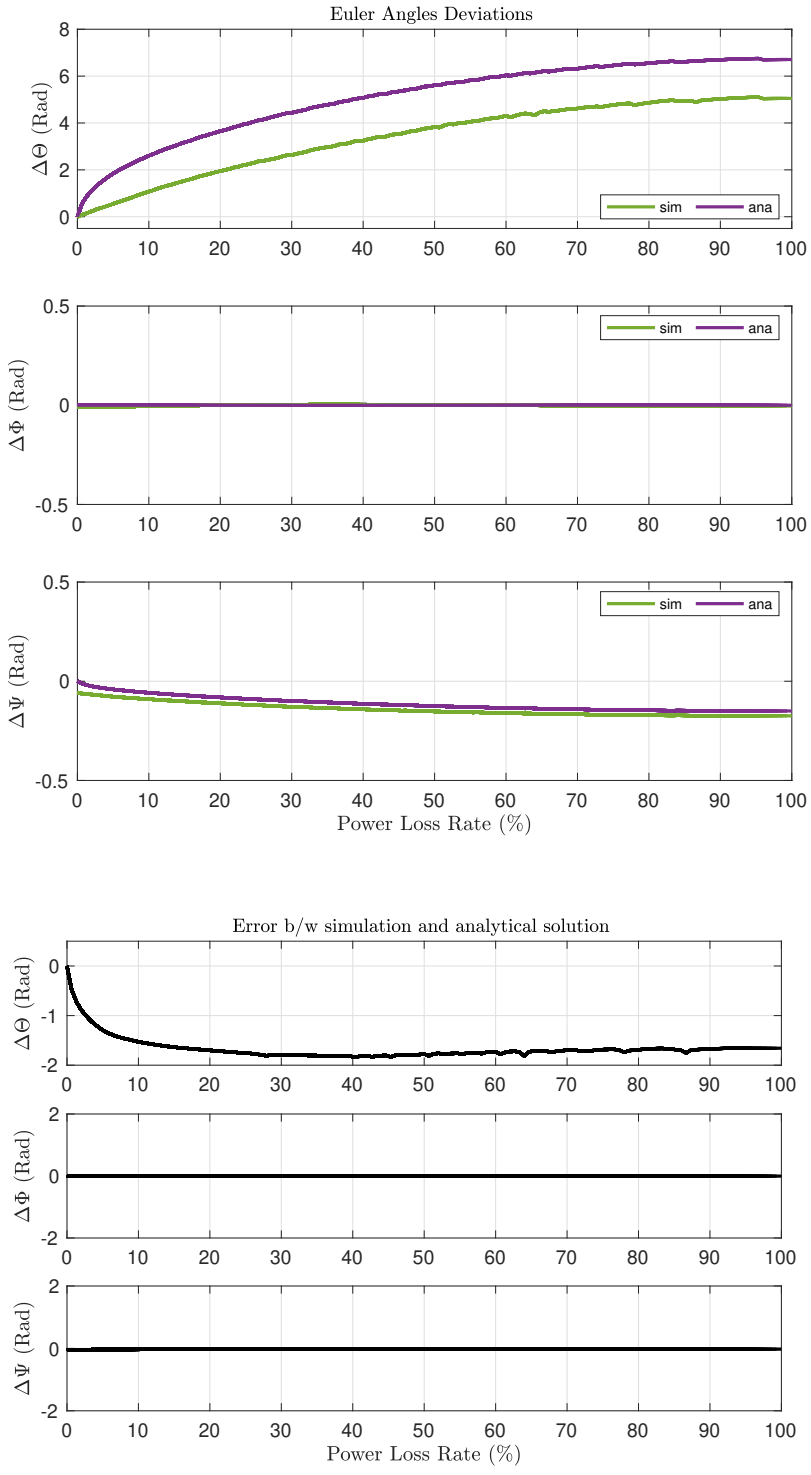

Figure 10. Euler angle deviations vs power loss of Rotor 1 in hovering flight and errors b/w simulation and analytical solution for scenario 1.

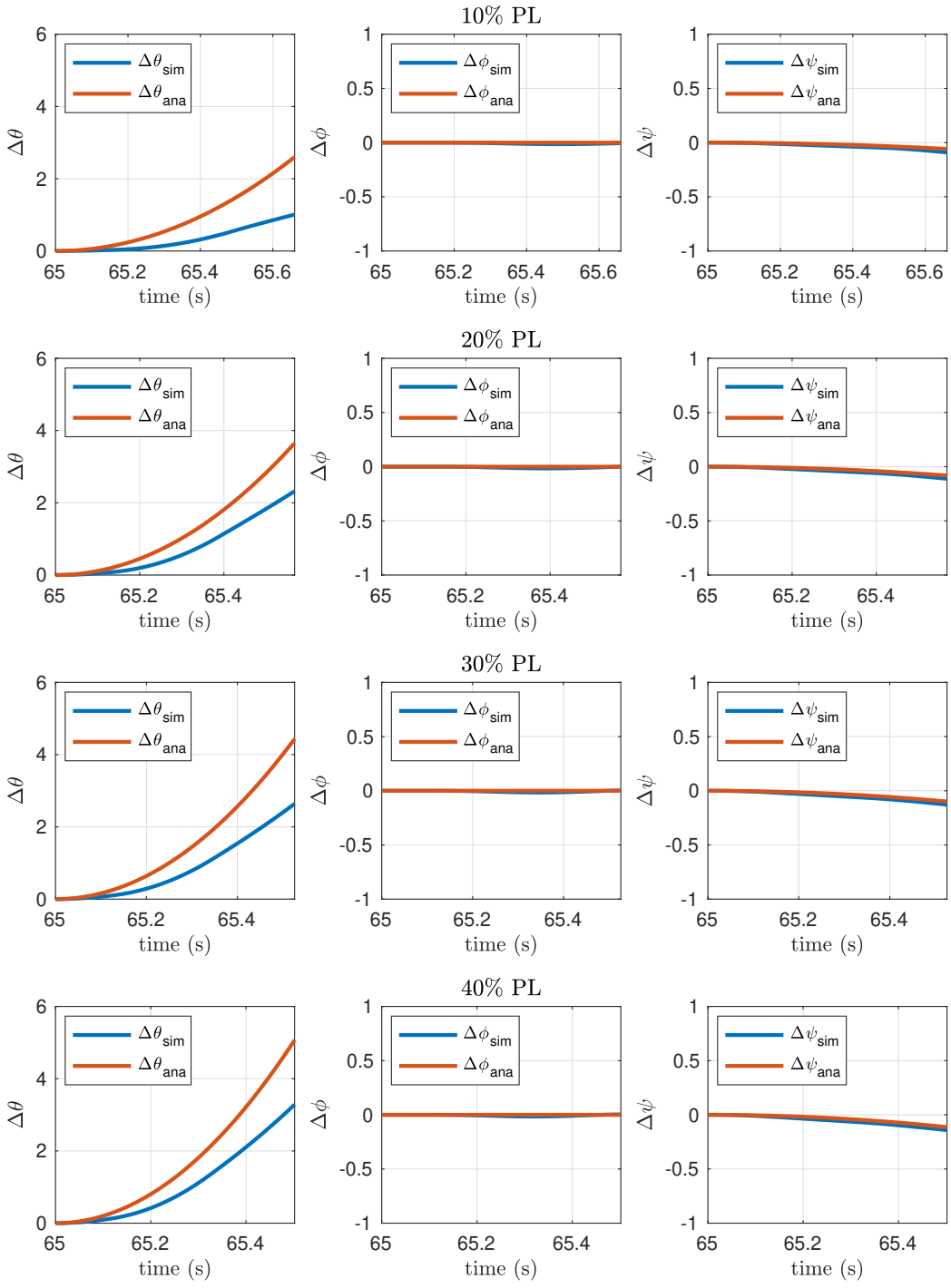

Figure 11. $\Delta\theta$, $\Delta\phi$ and $\Delta\psi$ deviations vs time with certain power loss rates of Rotor 1 for scenario 1.

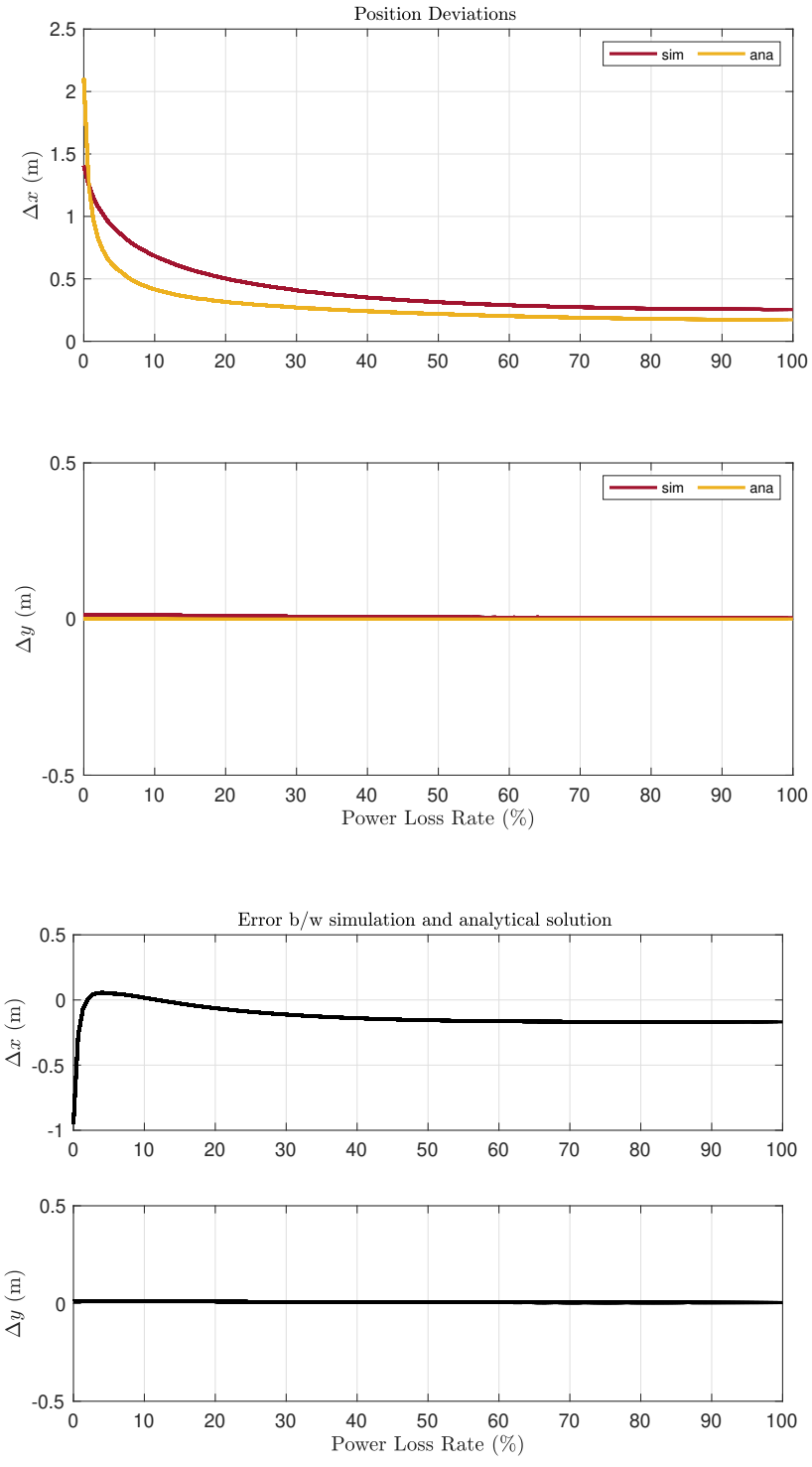

Figure 12. Position deviations vs power loss of Rotor 1 in hovering flight and errors b/w simulation and analytical solution for scenario 1 .

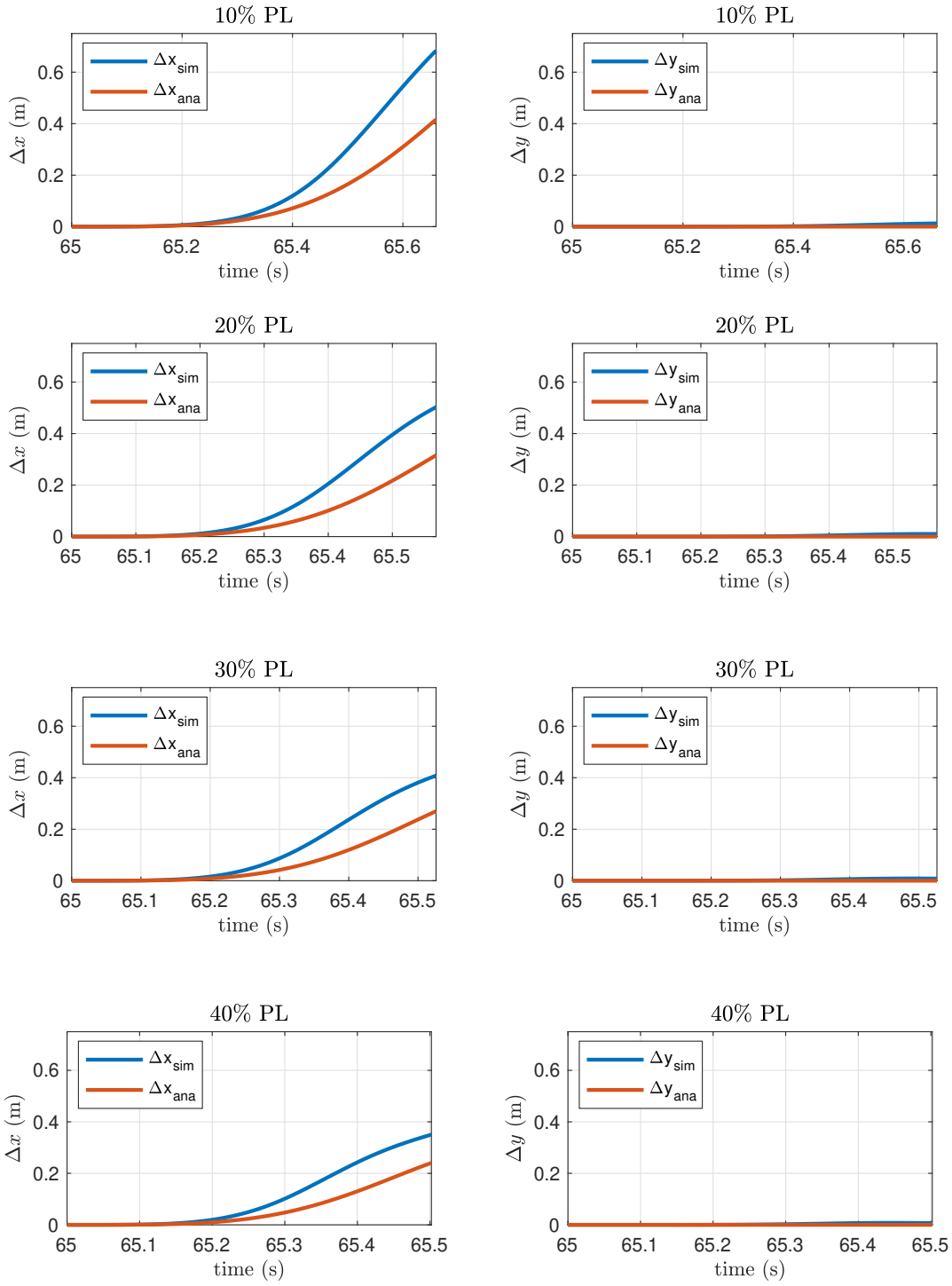

Figure 13. Δx and Δy deviations vs time with certain power loss rates of Rotor 1 for scenario 1.

5.3 Scenario 2 Results

It is assumed that the quadrotor's number 1 and 2 rotors are subjected to the same percent of power loss at the time of 65 s of hovering flight. The deviation trajectories are obtained based on the power loss rate and the impact zone is shown.

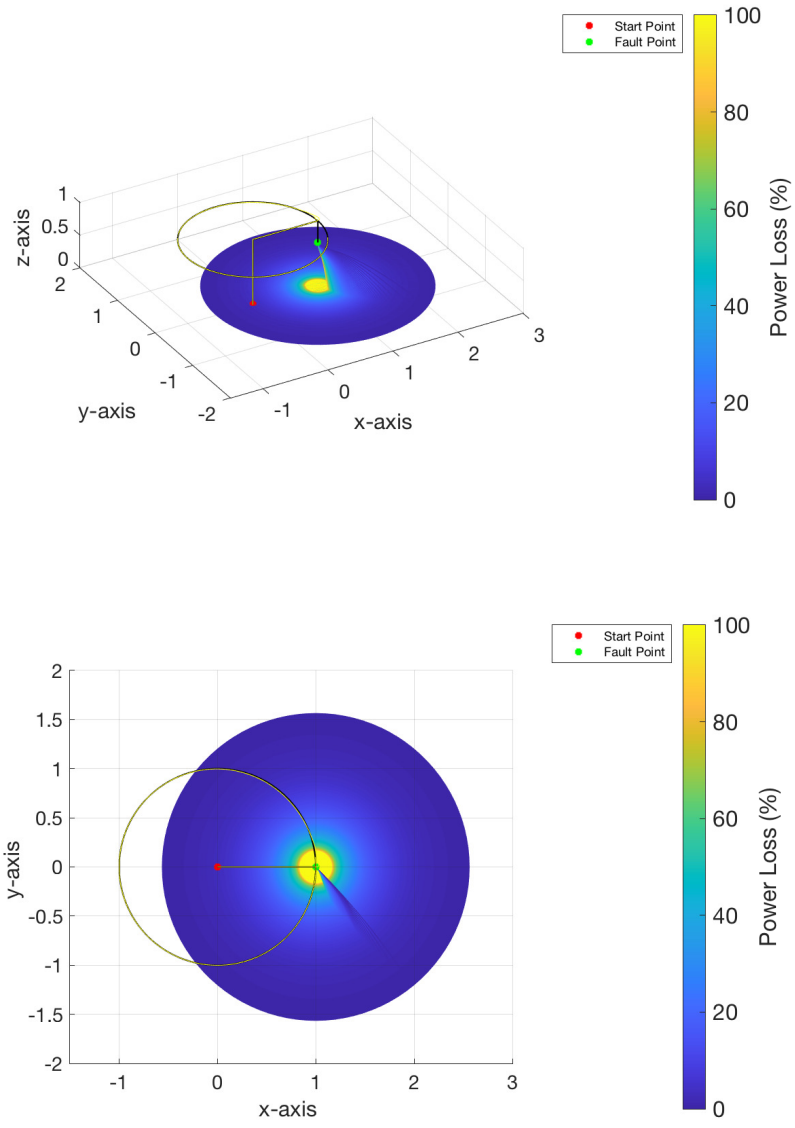

Figure 14. 3d and top views for crash zone in scenario 2.

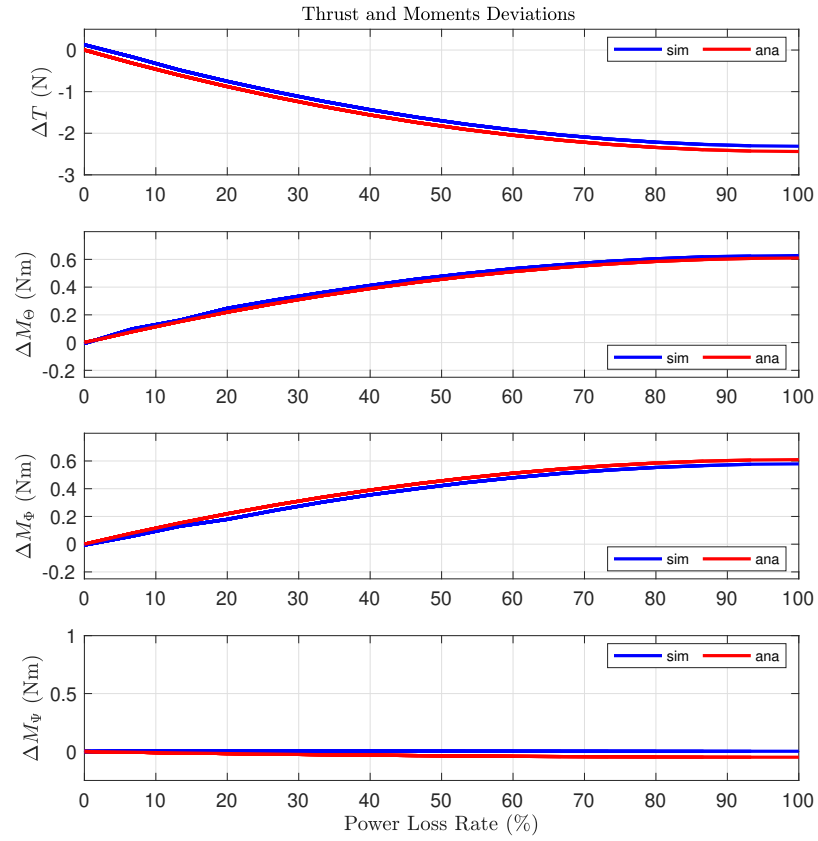

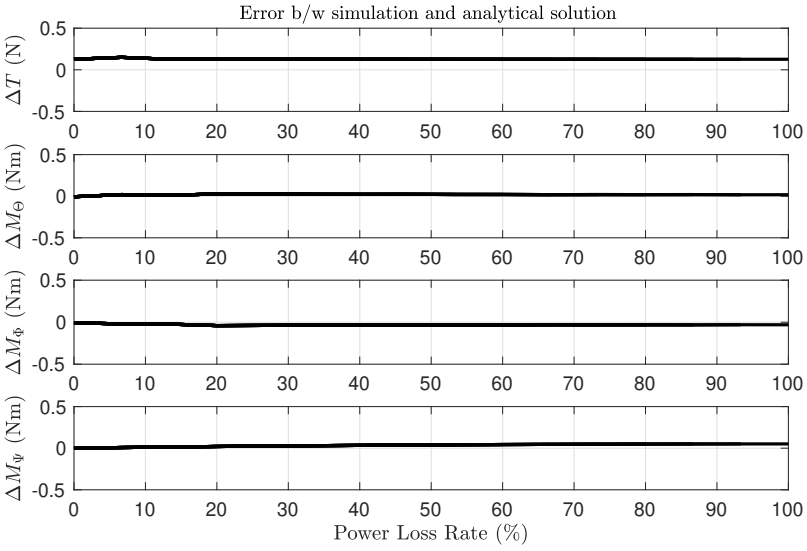

Figure 15. Thrust & moments deviations vs power loss of both Rotor 1&2 in hovering flight and errors b/w simulation and analytical solution for scenario 2 .

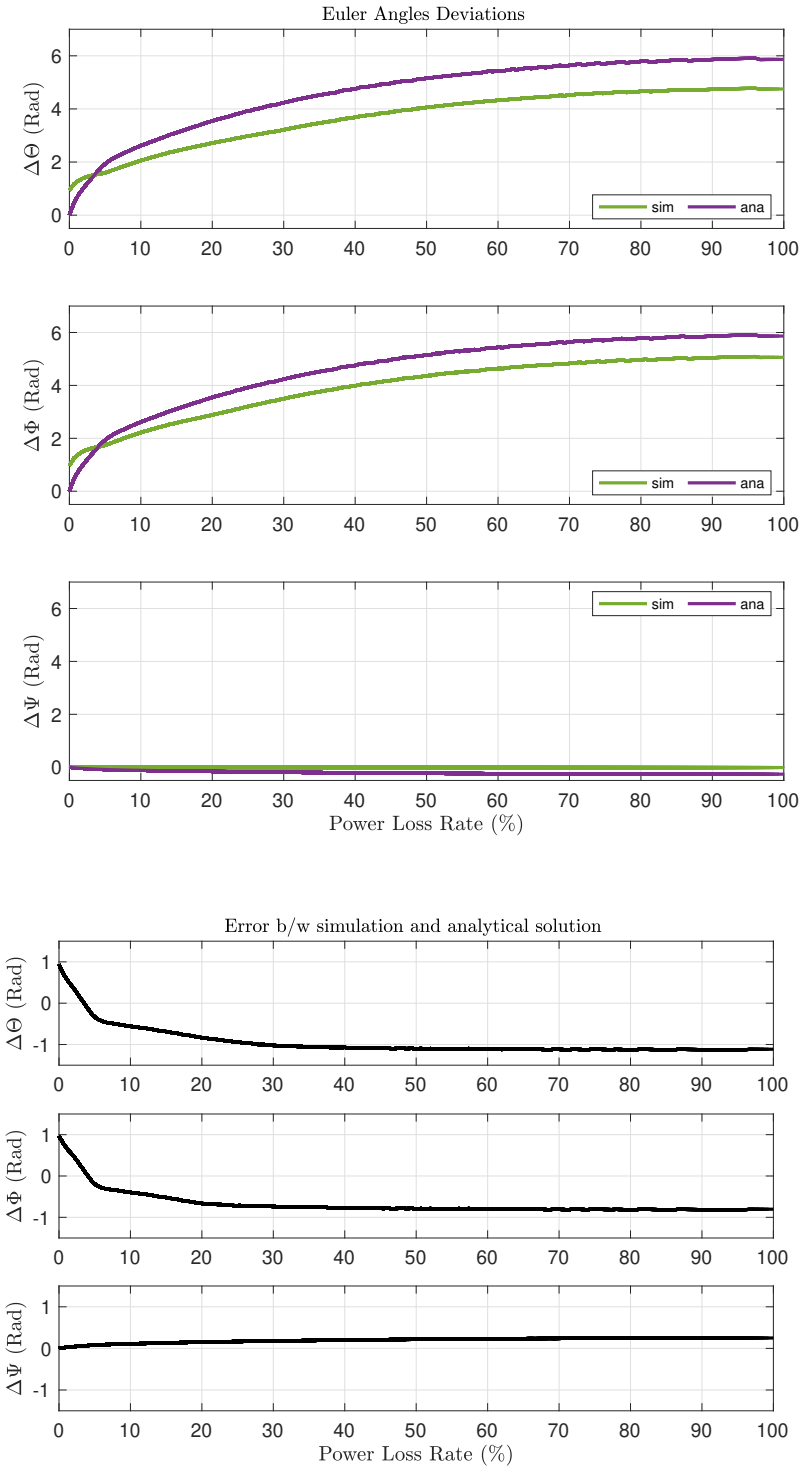

Figure 16. Euler angle deviations vs power loss of both Rotor 1&2 in hovering flight and errors b/w simulation and analytical solution for scenario 2 .

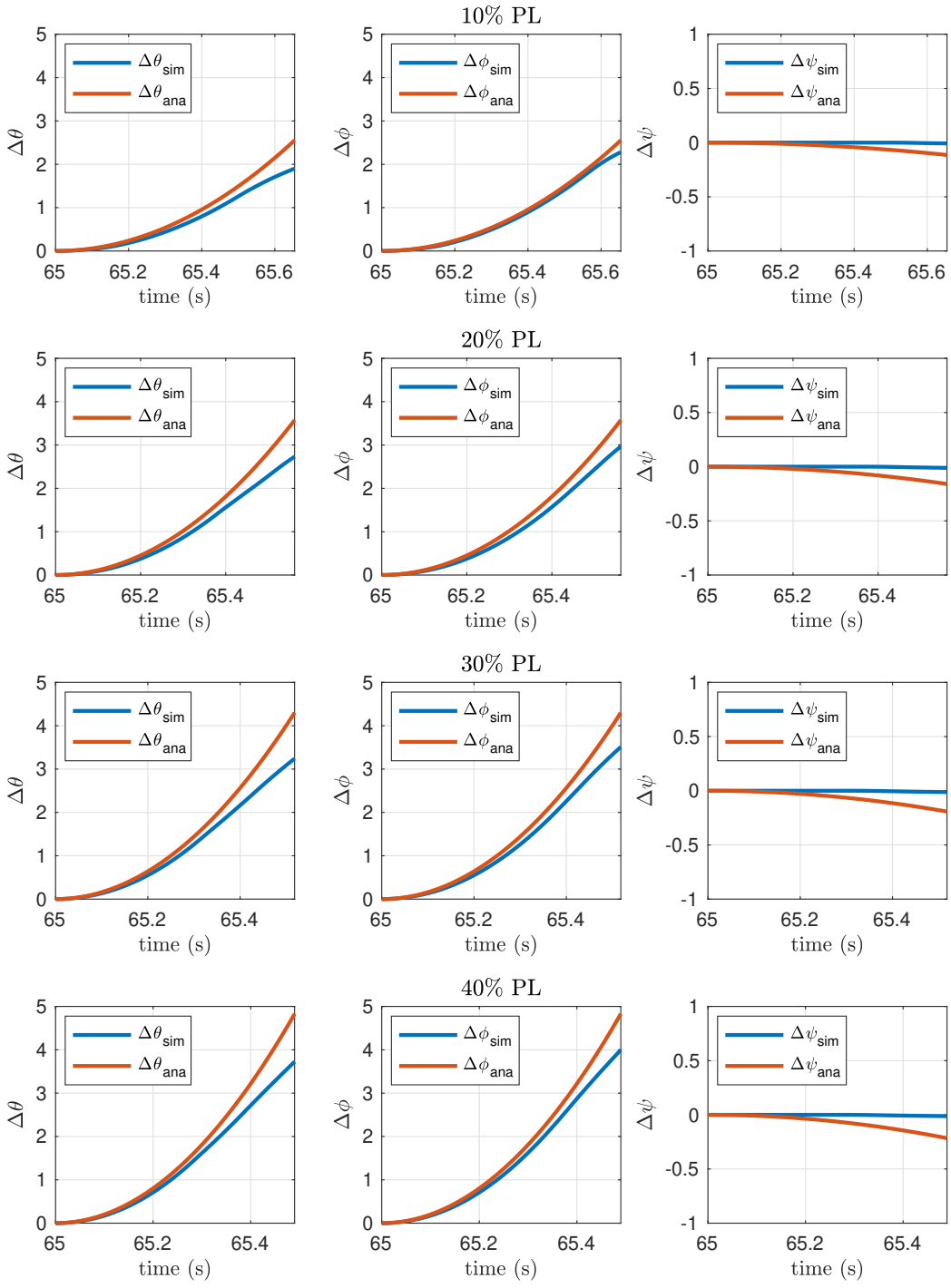

Figure 17. $\Delta\theta$, $\Delta\phi$ and $\Delta\psi$ deviations vs time with certain power loss rates of Rotor 1 and Rotor 2 for scenario 2.

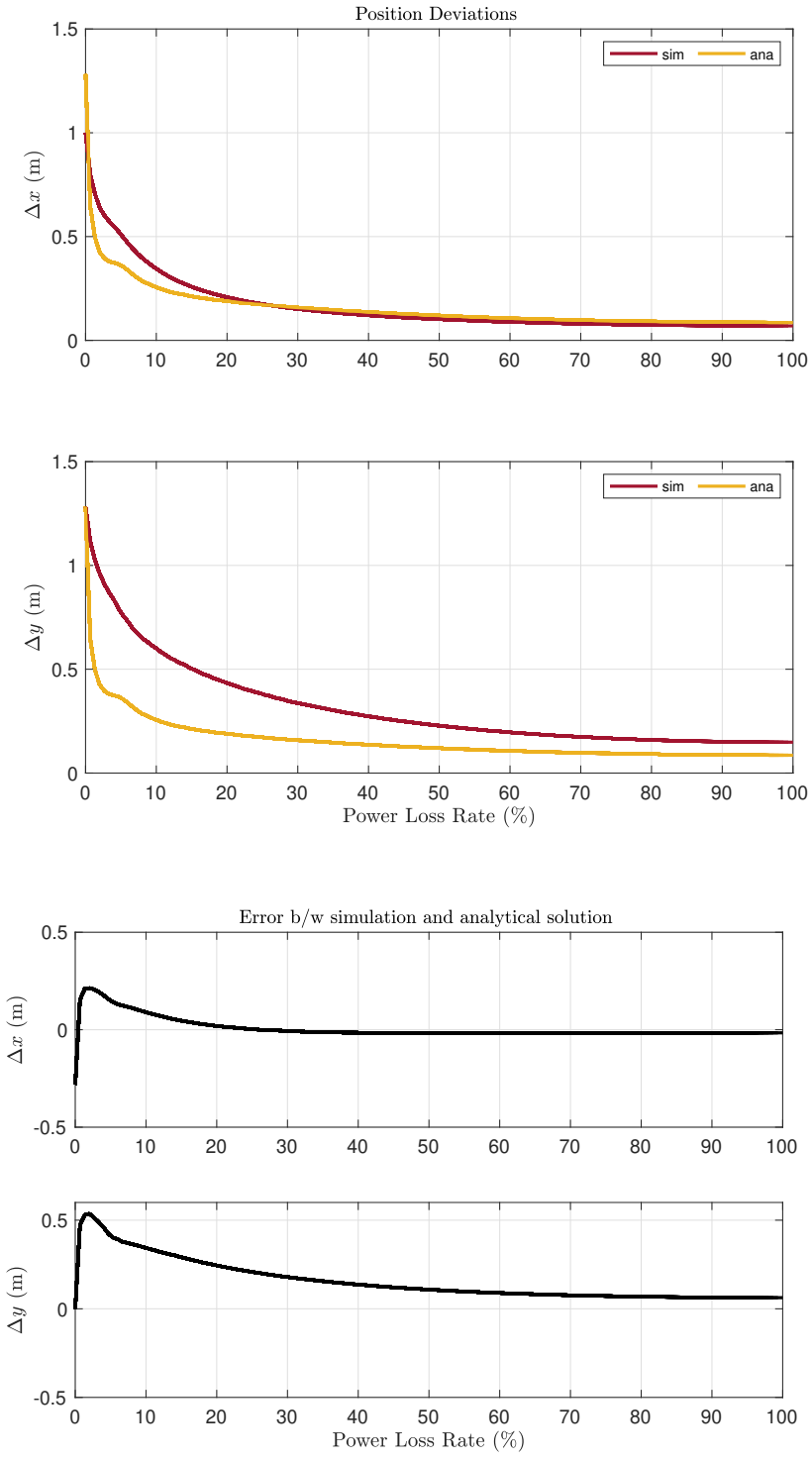

Figure 18. Position deviations vs power loss of both Rotor 1&2 in hovering flight and errors b/w simulation and analytical solution for scenario 2 .

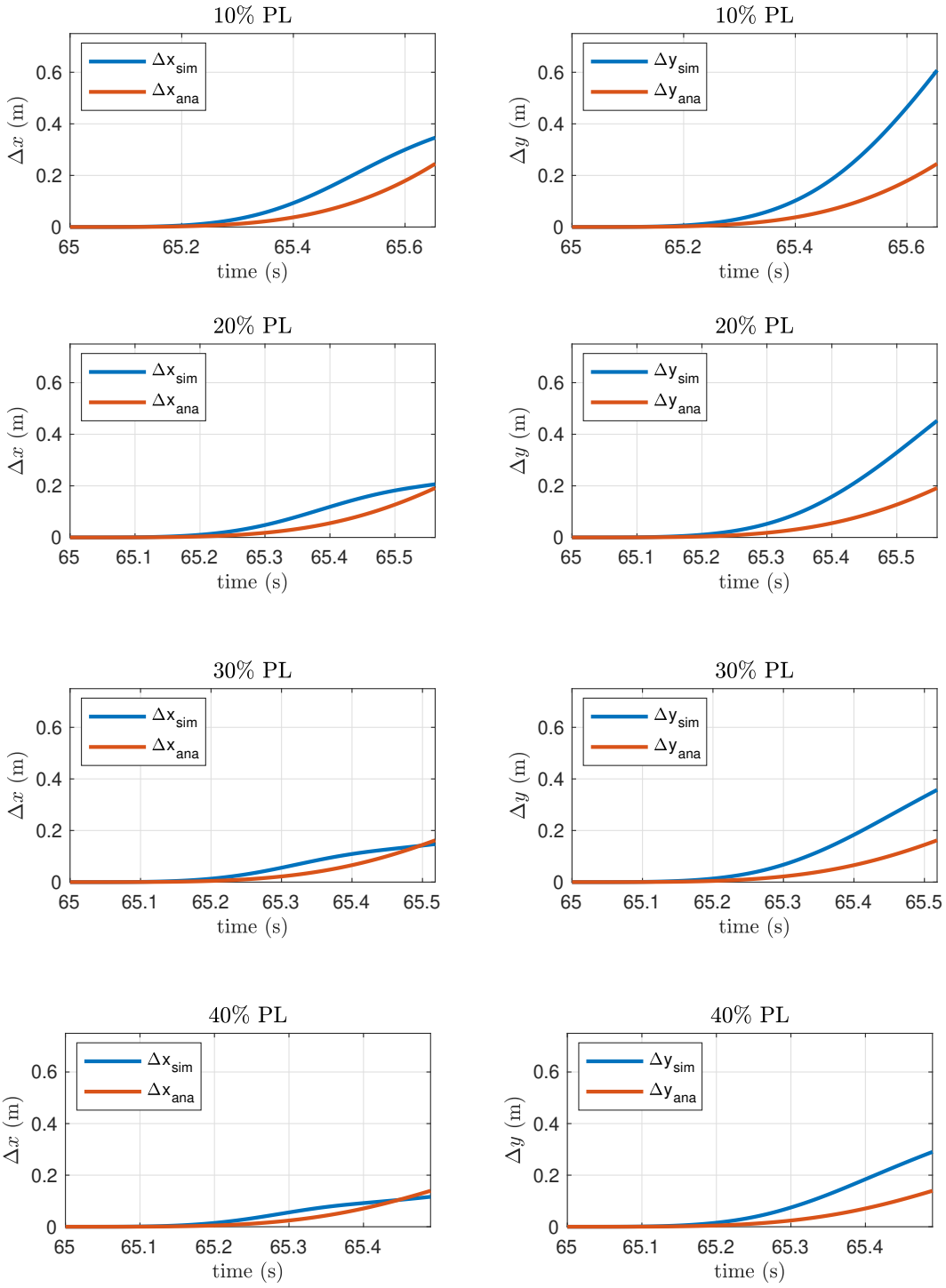

Figure 19. Δx and Δy deviations vs time with certain power loss rates of Rotor 1&2 for scenario 2.

5.4 Scenario 3 Results

It is assumed that the quadrotor's number 1 rotor is exposed the power loss at the time of 32 s of maneuvering flight. The deviation trajectories are obtained based on the power loss rate and the impact zone is shown.

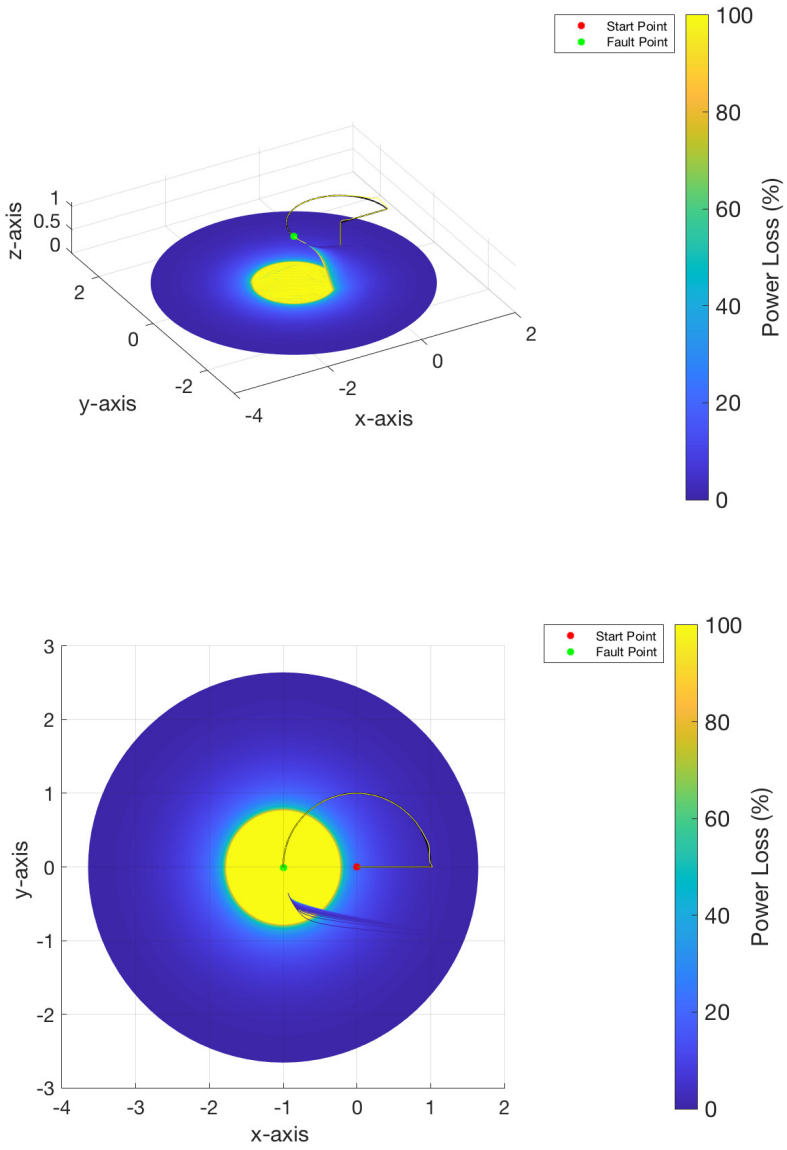

Figure 20. 3d and top views for crash zone in scenario 3.

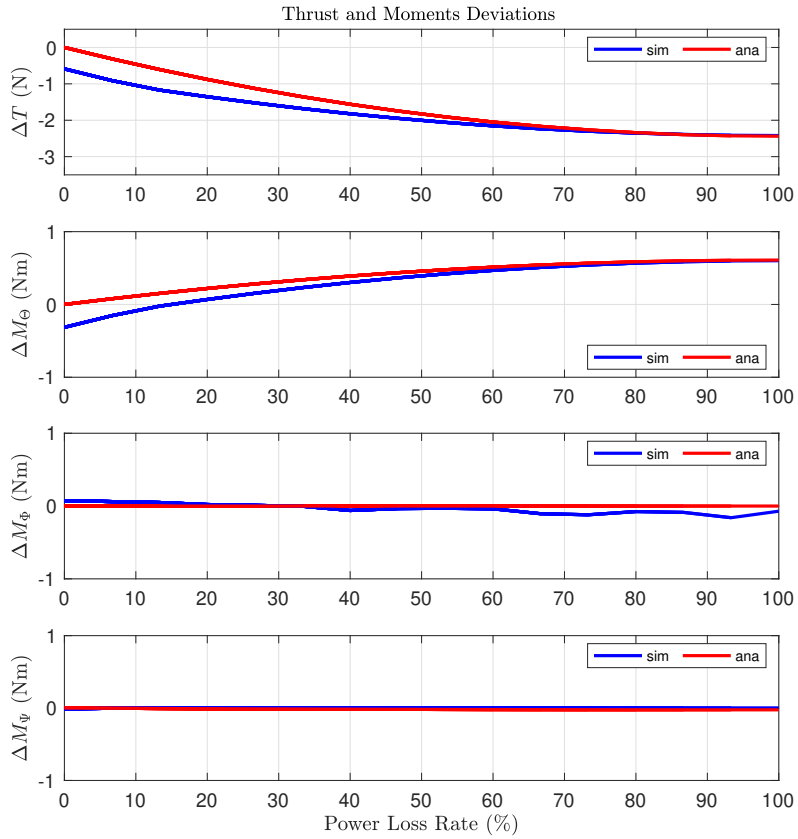

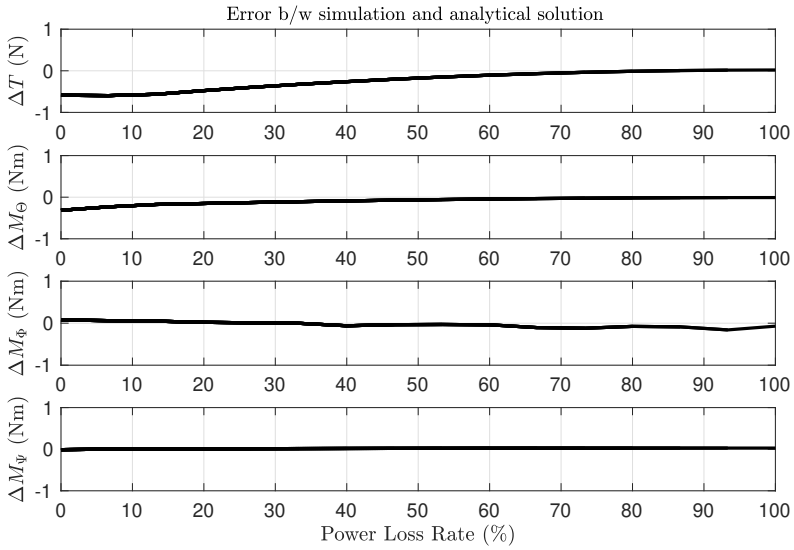

Figure 21. Thrust & moments deviations vs power loss of Rotor 1 in maneuvering flight and errors b/w simulation and analytical solution for scenario 3 .

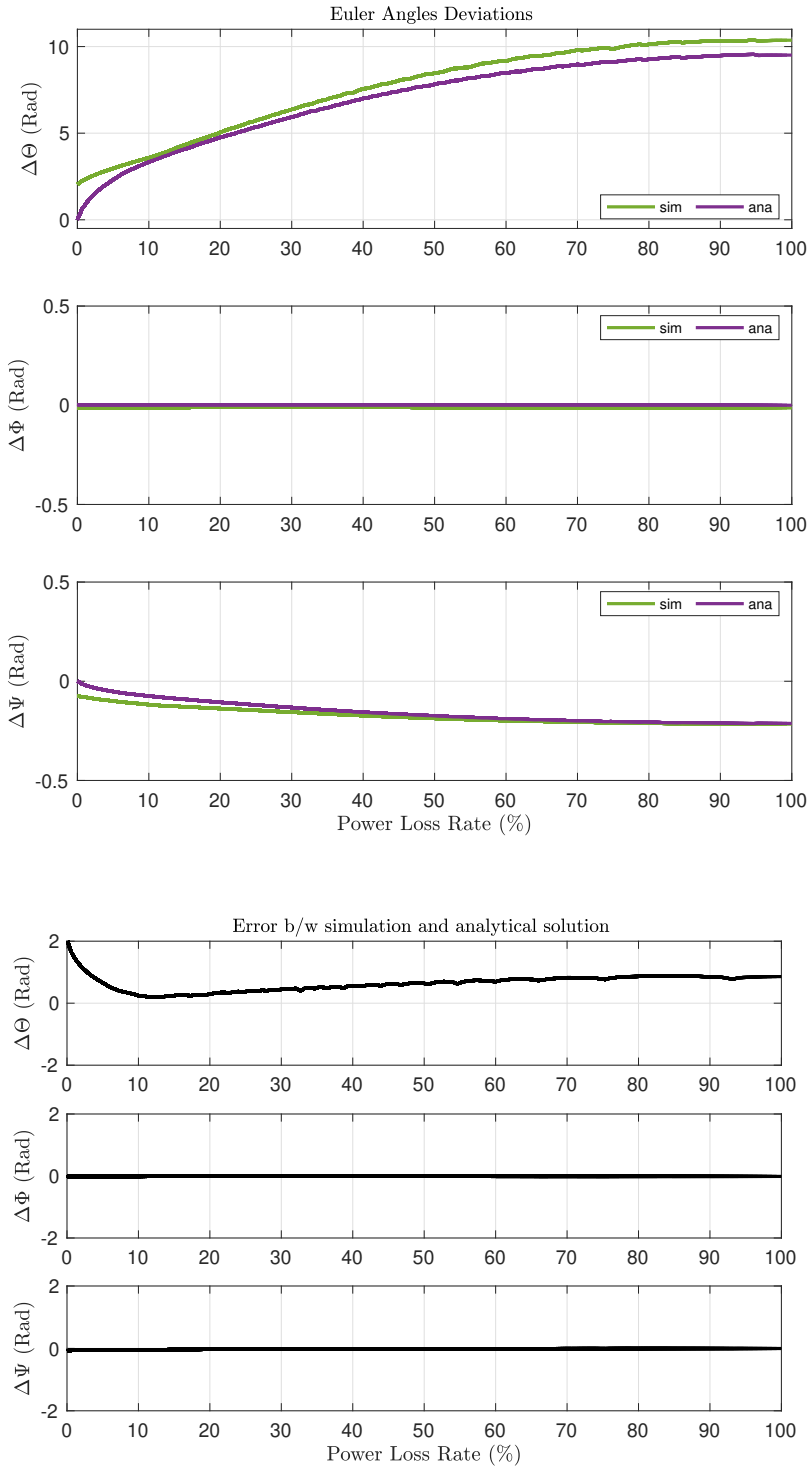

Figure 22. Euler angle deviations vs power loss of Rotor 1 in maneuvering flight and errors b/w simulation and analytical solution for scenario 3.

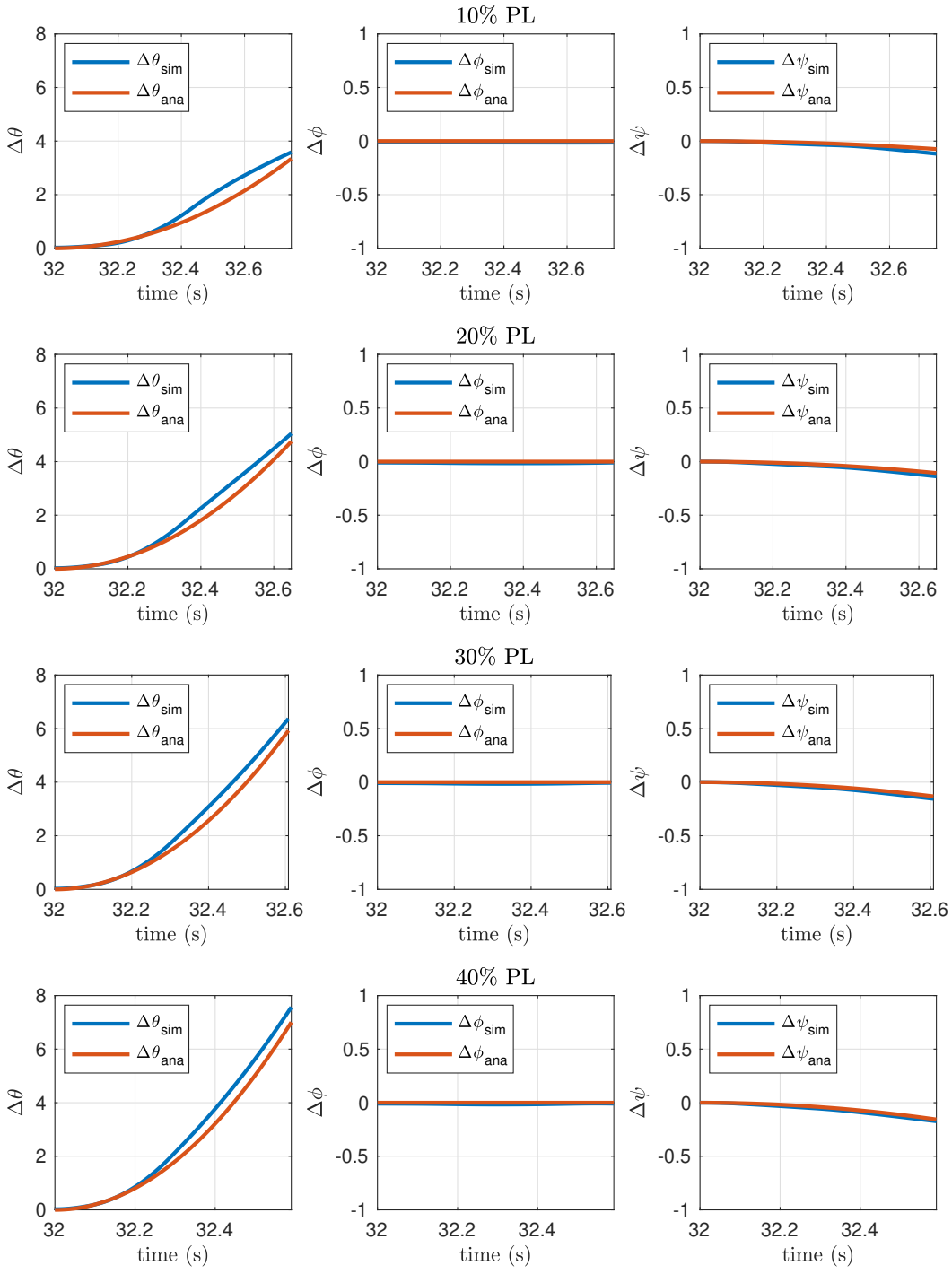

Figure 23. $\Delta\theta$, $\Delta\phi$ and $\Delta\psi$ deviations vs time with certain power loss rates of Rotor 1 for scenario 3.

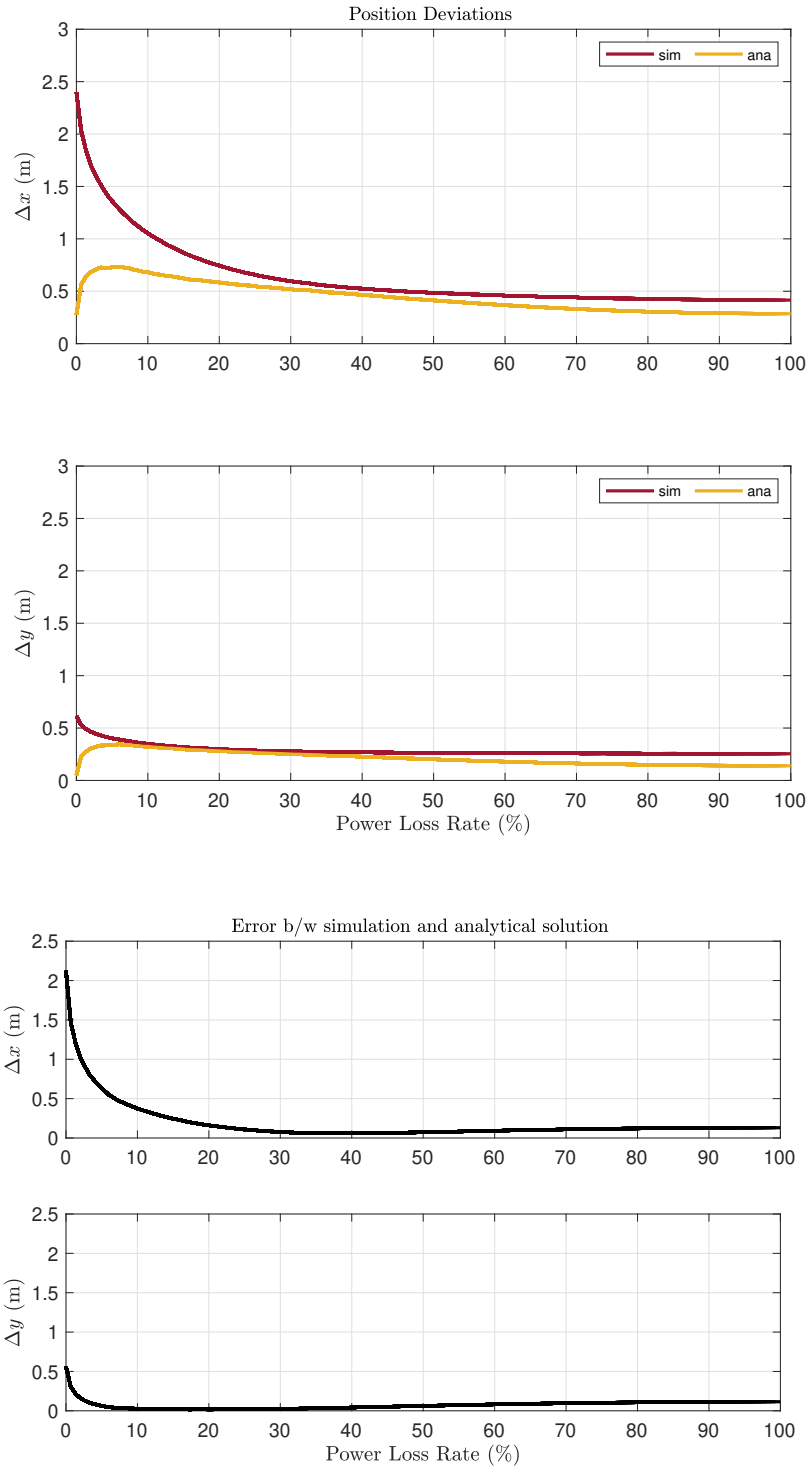

Figure 24. Position deviations vs power loss of Rotor 1 in maneuvering flight and errors b/w simulation and analytical solution for scenario 3 .

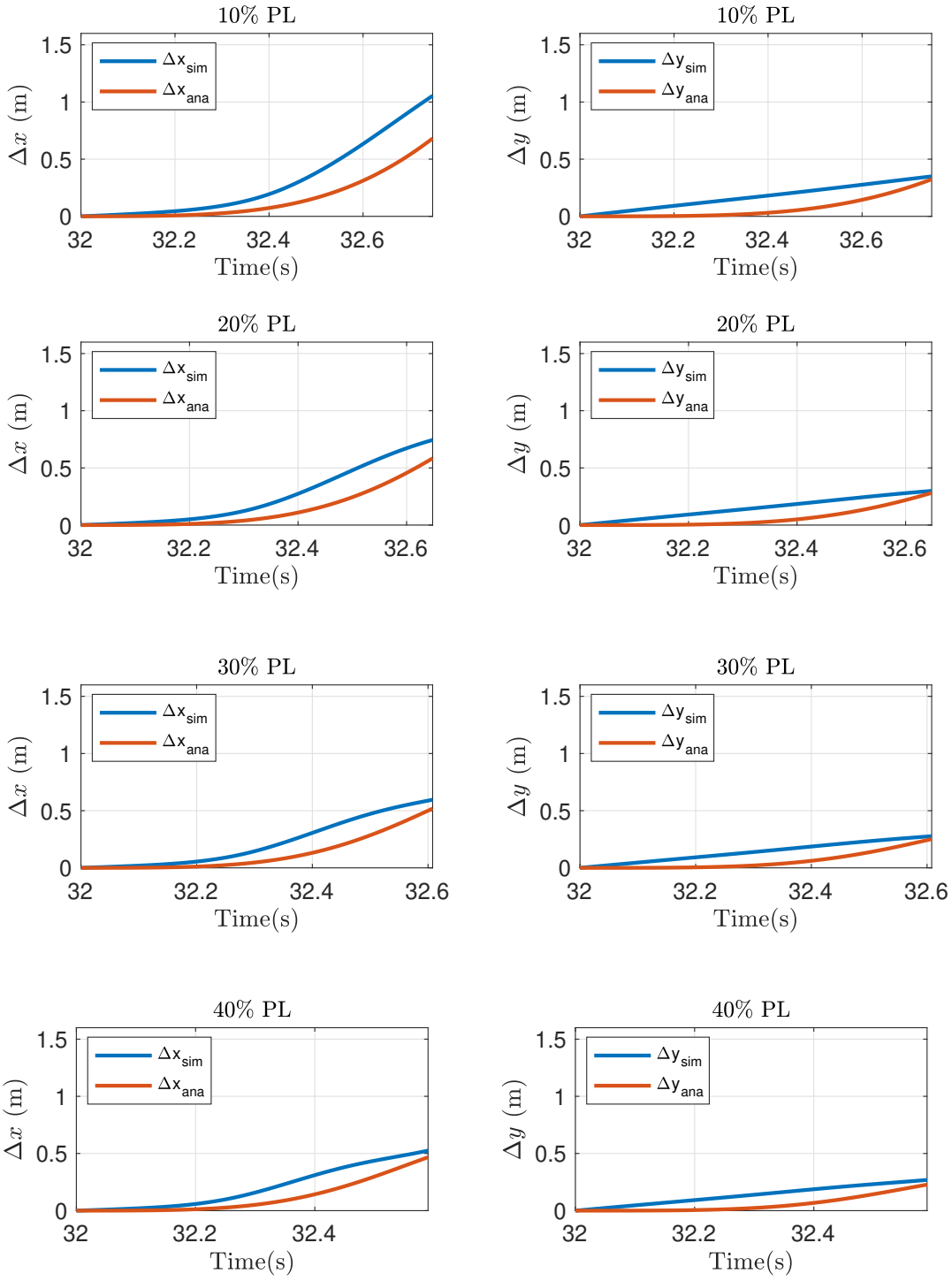

Figure 25. Δx and Δy deviations vs time with certain power loss rates of Rotor 1 for scenario 3.

5.5 Scenario 4 Results

It is assumed that the quadrotor's number 1 and 2 rotors are subjected to the same percent of power loss at the time of 32 s of maneuvering flight. The deviation trajectories are obtained based on the power loss rate and the impact zone is shown.

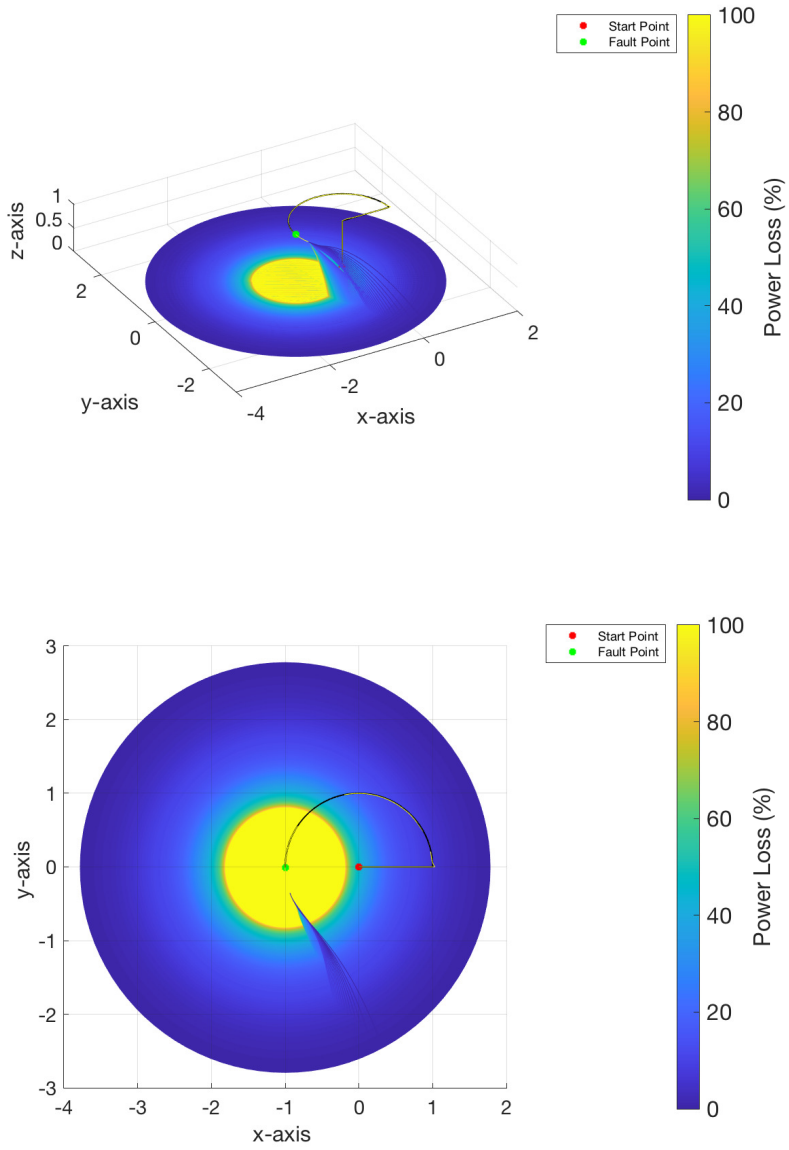

Figure 26. 3d and top views for crash zone in scenario 4.

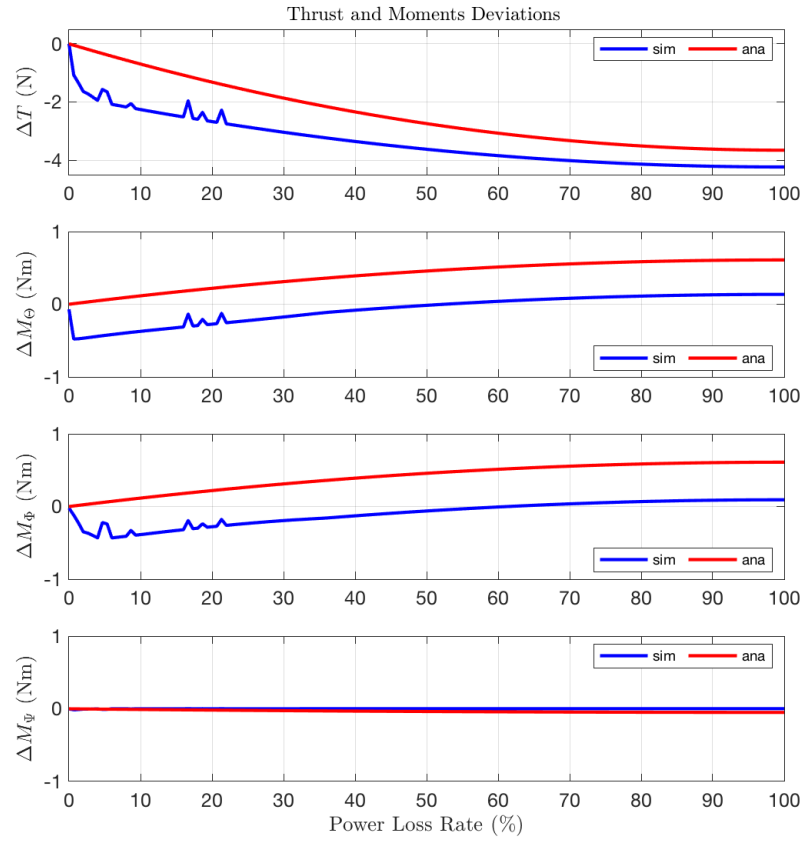

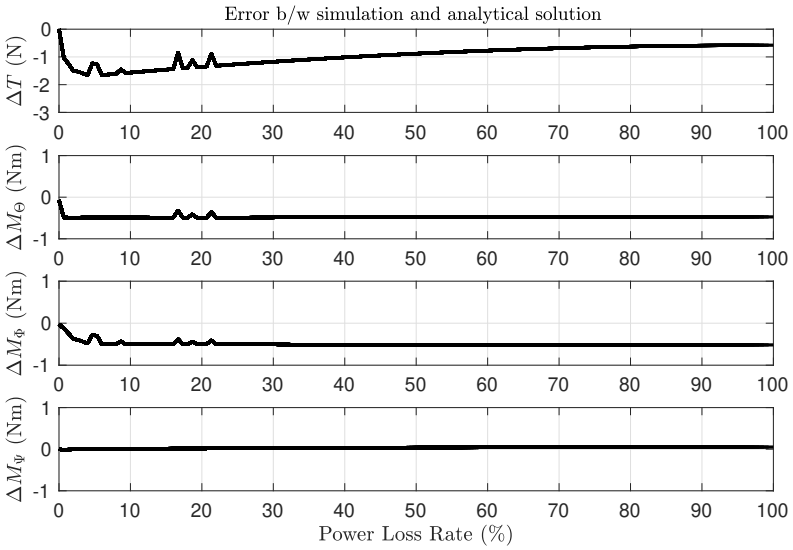

Figure 27. Thrust & moments deviations vs power loss of both Rotor 1&2 in maneuvering flight and errors b/w simulation and analytical solution for scenario 4 .

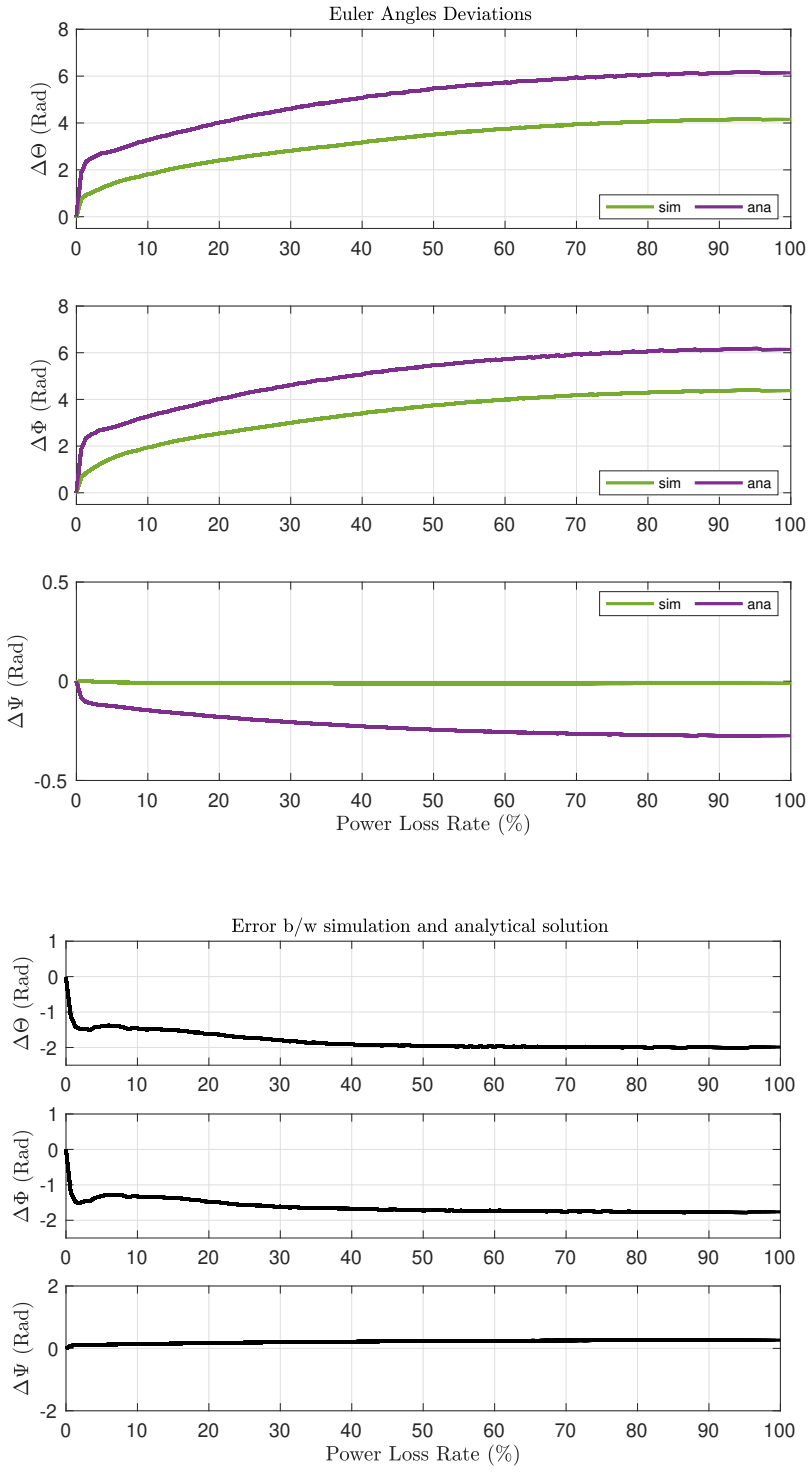

Figure 28. Euler angle deviations vs power loss of both Rotor 1&2 in maneuvering flight and errors b/w simulation and analytical solution for scenario 4 .

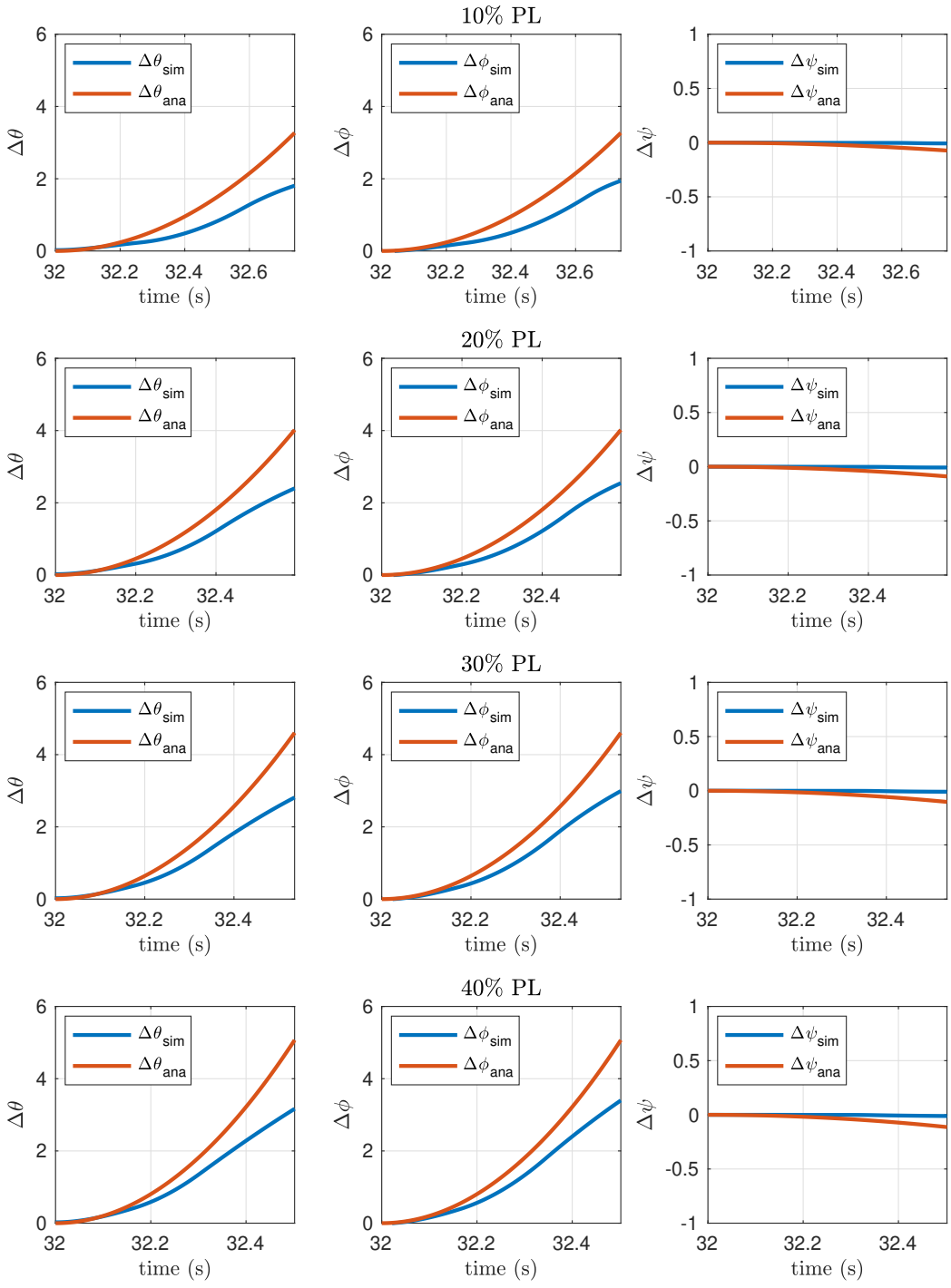

Figure 29. $\Delta\theta$, $\Delta\phi$ and $\Delta\psi$ deviations vs time with certain power loss rates of Rotor 1 and Rotor 2 for scenario 4.

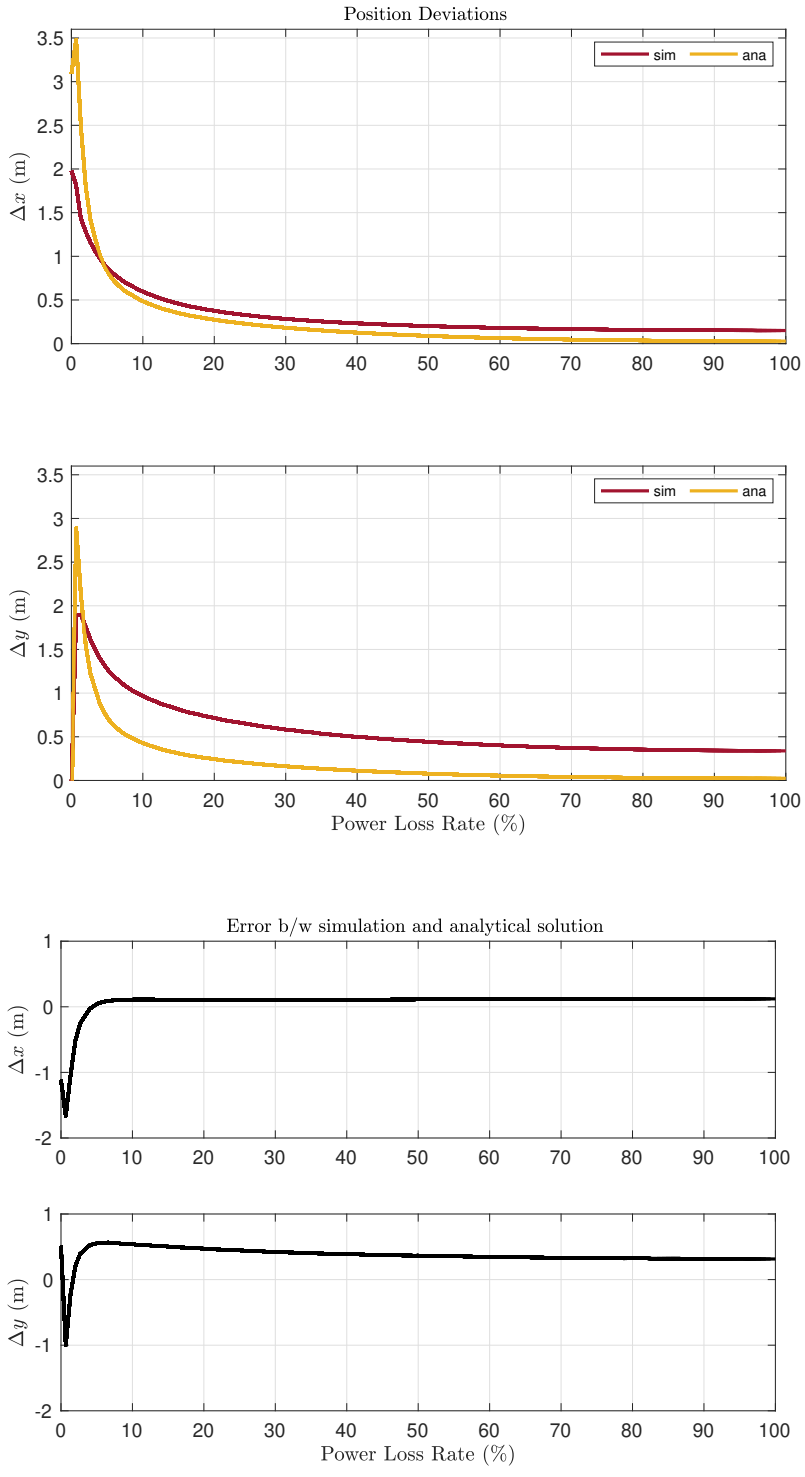

Figure 30. Position deviations vs power loss of both Rotor 1&2 in maneuvering flight and errors b/w simulation and analytical solution for scenario 4.

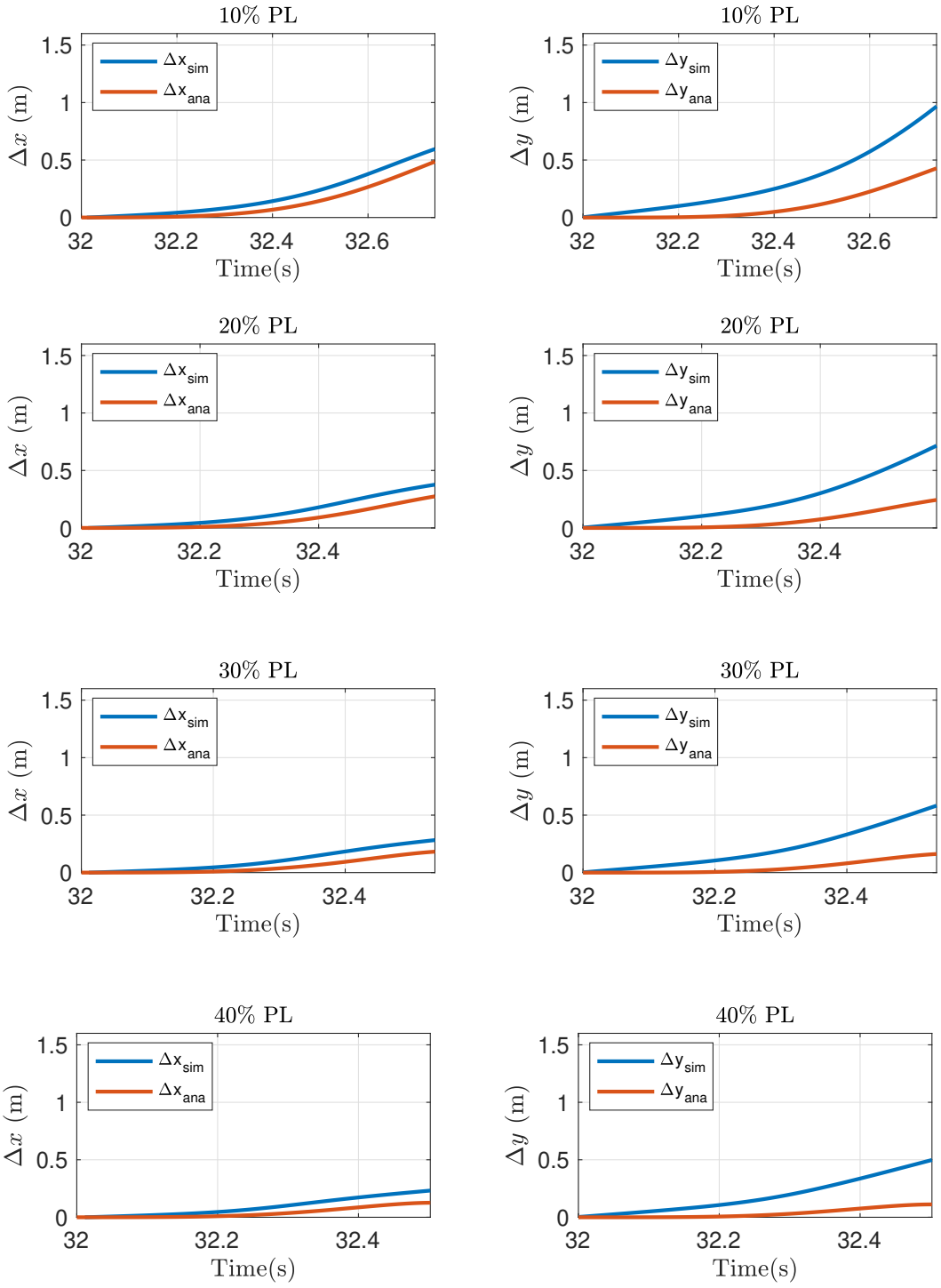

Figure 31. Δx and Δy deviations vs time with certain power loss rates of Rotor 1&2 for scenario 4.

CHAPTER 6

CONCLUSION

This thesis started with deriving the fundamental motion concepts and necessary mathematical basics to develop a quadrotor model. Then, the quadrotor's kinematic and dynamic equations were derived, considering certain assumptions. Because the quadrotor platform is a highly nonlinear system, a nonlinear control approach called dynamic inversion was utilized to attain good flight performance. This control method can be accepted as a linearization procedure that was obtained algebraically a coordinate transformation of nonlinear states. Thus, a linear feedback law between inputs and outputs can be obtained by canceling nonlinearities of the system. The designed controller was tested in 3d circular trajectory and it can be seen that the quadrotor system followed the trajectory with a small amount of error.

In the second part of the thesis, the failure scenarios were developed to obtain a crash radius. Because quadrotor platforms may cause severe risk factors in the urban areas, this impact region must be defined to obtain an appropriate flying path. The failure scenarios are based on the power loss of rotor faults due to considering physical damages. Then, faulted rotors' power loss information was utilized to find the deviation on horizontal axes and the possible crash circle radius. Thus, the crash zone can be calculated with the situation of the potential rotor failures. The results illustrated that the simulation and analytical approach outcomes are close to each other.

REFERENCES

[1] S. Bouabdallah. Design and control of quadrotors with application to autonomous flying. 2007.

[2] S. Bouabdallah, A. Noth, and R. Siegwart. Pid vs lq control techniques applied to an indoor micro quadrotor. 3:2451–2456 vol.3, 2004.

[3] S. Bouabdallah and R. Siegwart. Backstepping and sliding-mode techniques applied to an indoor micro quadrotor. pages 2247–2252, 2005.

[4] S. Bouabdallah and R. Siegwart. Full control of a quadrotor. pages 153–158, 2007.

[5] H. Bouadi and F. Mora-Camino. Direct adaptive backstepping flight control for quadcopter trajectory tracking. pages 1–8, 2018.

[6] Y. Bouzid, H. Siguerdidjane, and Y. Bestaoui. Boosted flight controller for quadrotor navigation under disturbances. *IFAC-PapersOnLine*, 50(1):10293–10298, 2017.

[7] I. Choi and H. Bang. Quadrotor-tracking controller design using adaptive dynamic feedback-linearization method. *Proceedings of the Institution of Mechanical Engineers, Part G: Journal of Aerospace Engineering*, 228(12):2329–2342, 2014.

[8] I. D. Cowling, O. A. Yakimenko, J. F. Whidborne, and A. K. Cooke. A prototype of an autonomous controller for a quadrotor uav. pages 4001–4008, 2007.

[9] A. Das, F. Lewis, and K. Subbarao. Backstepping approach for controlling a quadrotor using lagrange form dynamics. *Journal of Intelligent and Robotic Systems*, 56(1-2):127–151, 2009.

[10] A. Das, K. Subbarao, and F. Lewis. Dynamic inversion with zero-dynamics stabilisation for quadrotor control. *IET control theory & applications*, 3(3):303–314, 2009.

[11] B. Erginer and E. Altug. Modeling and pd control of a quadrotor vtol vehicle. *2007 IEEE Intelligent Vehicles Symposium*, pages 894–899, 2007.

[12] S. W. G. Hoffmann, H. Huang and C. Tomlin. Quadrotor helicopter flight dynamics and control: Theory and experiment. *AIAA Guidance, Navigation and Control Conference and Exhibit, Aug. 2007*, pages 10.2514/6.2007–6461, 2007.

[13] J. Ghandour, S. Aberkane, and J.-C. Ponsart. Feedback linearization approach for standard and fault tolerant control: Application to a quadrotor UAV testbed. *Journal of Physics: Conference Series*, 570(8):082003, dec 2014.

[14] S. Grzonka, G. Grisetti, and W. Burgard. A fully autonomous indoor quadrotor. *IEEE Transactions on Robotics*, 28(1):90–100, 2012.

[15] Y. Kartal, P. Kolaric, V. Lopez, A. Dogan, and F. Lewis. Backstepping approach for design of pid controller with guaranteed performance for micro-air uav. *Control Theory and Technology*, pages 1–15, 2019.

[16] D.-W. Lee, H. J. Kim, and S. Sastry. Feedback linearization vs. adaptive sliding mode control for a quadrotor helicopter. *International Journal of Control, Automation and Systems*, 7:419–428, 2009.

[17] K. Lee, H. Kim, J. Park, and Y. Choi. Hovering control of a quadrotor. In *ICCAS 2012 - 2012 12th International Conference on Control, Automation and Systems*, International Conference on Control, Automation and Systems, pages 162–167, 2012. Copyright: Copyright 2013 Elsevier B.V., All rights reserved.; 2012 12th International Conference on Control, Automation and Systems, ICCAS 2012 ; Conference date: 17-10-2012 Through 21-10-2012.

[18] J. Li and Y. Li. Dynamic analysis and pid control for a quadrotor. *2011 IEEE International Conference on Mechatronics and Automation*, pages 573–578, 2011.

[19] T. Li, Y. Zhang, and B. W. Gordon. Nonlinear fault-tolerant control of a quadrotor uav based on sliding mode control technique. *IFAC Proceedings Volumes*, 45(20):1317–1322, 2012.

[20] T. Madani and A. Benallegue. Backstepping control for a quadrotor helicopter. *2006 IEEE/RSJ International Conference on Intelligent Robots and Systems*, pages 3255–3260, 2006.

[21] T. Madani and A. Benallegue. Control of a quadrotor mini-helicopter via full state backstepping technique. *Proceedings of the 45th IEEE Conference on Decision and Control*, pages 1515–1520, 2006.

[22] L. D. Minh and C. Ha. Modeling and control of quadrotor mav using vision-based measurement. *International Forum on Strategic Technology 2010*, pages 70–75, 2010.

[23] P. Pounds, R. Mahony, and P. Corke. Modelling and control of a large quadrotor robot. *Control Engineering Practice*, 18(7):691 – 699, 2010. Special Issue on Aerial Robotics.

[24] Zhi Li, Xin Ma, Zhigang Xu, Yafang Wang, and Yibin Li. Chattering free sliding adaptive attitude control for quadrotor. pages 707–712, 2016.

[25] M. Önder Efe and S. Member. Neural network assisted computationally simple pid control of a quadrotor uav.

BIOGRAPHICAL STATEMENT

Ahmet Tolcu was born in Kayseri, Turkey. He received his bachelor's degrees in Mechatronics Engineering and Electrical-Electronics Engineering from Erciyes University in 2014 and 2015. He worked for Dener Machinery as an engineer in the Laser CNC Department after graduation.

He is receiving his Master of Science degree in Aerospace Engineering at the University of Texas at Arlington, in which the Republic of Turkey Ministry of National Education sponsored him to study in the field of aerospace. His research interests include advanced dynamics and control of autonomous systems.